Defense Threat Reduction Agency
8725 John J. Kingman Road, MS 6201
Fort Belvoir, VA 22060-6201

DTRA-TR-04-24

TECHNICAL REPORT

Modeling and Characterization of Microbarom Signals in the Pacific

Approved for public release; distribution is unlimited.

September 2006

DTRA 01-01-C-0077

Milton Garces
Mark Willis

Prepared by:
University of Hawaii, Monoa
Infrasound Laboratory
73-4460 Queen Kaahumanu Hwy., #119
Kailua-Kona, HI 96740-2638

DESTRUCTION NOTICE

FOR CLASSIFIED documents, follow the procedures in DoD 5550.22-M, National Industrial Security Program Operating Manual, Chapter 5, Section 7 (NISPOM) or DoD 5200.1-R, Information Security Program Regulation, Chapter 1X.

FOR UNCLASSIFIED limited documents, destroyed by any method that will prevent disclosure of contents or reconstruction of the document.

Retention of this document by DoD contractors is authorized in accordance with DoD 5220.22M, Industrial Security manual.

PLEASE NOTIFY THE DEFENSE THREAT REDUCTION AGENCY, ATTN: IMMI, 8725 JOHN J. KINGMAN ROAD, MS-6201, FT. BELVOIR, VA 22060-6201. IF YOUR ADDRESS IS INCORRECT, IF YOU WISH IT DELETED FROM THE DISTRIBUTION LIST, OR IF THE ADDRESSEE IS NO LONGER EMPLOYED BY YOUR ORGANIZATION.

DISTRIBUTION LIST UPDATE

This mailer is provided to enable DTRA to maintain current distribution lists for reports. (We would appreciate you providing the requested information.)

- ☐ Add the individual listed to your distribution list.
- ☐ Delete the cited organization/individual.
- ☐ Change of address.

Note:
Please return the mailing label from the document so that any additions, changes, corrections or deletions can be made easily. For distribution cancellation or more information call DTRA/BDMI (703) 767-4724.

NAME: _____

ORGANIZATION: _____

OLD ADDRESS	NEW ADDRESS
_____	_____
_____	_____
_____	_____

TELEPHONE NUMBER: ( ) _____

DTRA PUBLICATION NUMBER/TITLE	CHANGES/DELETIONS/ADDITONS, etc. *(Attach Sheet if more Space is Required)*
_____	_____
_____	_____
_____	_____

DTRA or other GOVERNMENT CONTRACT NUMBER: _____

CERTIFICATION of NEED-TO-KNOW BY GOVERNMENT SPONSOR (if other than DTRA):

SPONSORING ORGANIZATION: _____

CONTRACTING OFFICER or REPRESENTATIVE: _____

SIGNATURE: _____

DEFENSE THREAT REDUCTION AGENCY
ATTN: BDLMI
8725 John J Kingman Road, MS 6201
Fort Belvoir, VA 22060-6201

DEFENSE THREAT REDUCTION AGENCY
ATTN: BDLMI
8725 John J Kingman Road, MS 6201
Fort Belvoir, VA 22060-6201

REPORT DOCUMENTATION PAGE

Form Approved
OMB No. 0704-0188

1. REPORT DATE *(DD-MM-YYYY)*	2. REPORT TYPE	3. DATES COVERED *(From - To)*
00-09-2006	Technical Report	

4. TITLE AND SUBTITLE

Modeling and Characterization of Microbarom Signals in the Pacific

5a. CONTRACT NUMBER
DTRA 01-01-C-0077

5b. GRANT NUMBER

5c. PROGRAM ELEMENT NUMBER
YYY4

6. AUTHOR(S)

Milton Garces and Mark Willis

5d. PROJECT NUMBER
OH

5e. TASK NUMBER
OO

5f. WORK UNIT NUMBER
DH99040

7. PERFORMING ORGANIZATION NAME(S) AND ADDRESS(ES)

University of Hawaii, Monoa
Infrasound Laboratory
73-4460 Queen Kaahumanu Hwy., #119
Kailua-Kona, HI 96740-2638

8. PERFORMING ORGANIZATION REPORT NUMBER

9. SPONSORING / MONITORING AGENCY NAME(S) AND ADDRESS(ES)
Defense Threat Reduction Agency
8725 John J. Kingman Rd., MS 6201
Fort Belvoir, VA 22060-6201

TDND / D. Barber

10. SPONSOR/MONITOR'S ACRONYM(S)

11. SPONSOR/MONITOR'S REPORT NUMBER(S)

12. DISTRIBUTION / AVAILABILITY STATEMENT

Approved for public release; distribution is unlimited.

13. SUPPLEMENTARY NOTES

This work was sponsored by the Defense Threat Reduction Agency under RDT&E RMC code B YYY4 C 5000 OH OO 99040 25904 D.

14. ABSTRACT

Naturally occurring sources of infrasound include (but are not limited to) severe weather, volcanoes, bolides, earthquakes, surf, mountain waves, and, the focus of this research, nonlinear ocean wave interactions. Man-made sources of infrasound also exist, such as airplane activity, military testing, rocket launches, and nuclear explosions (Bedard and Georges, 2000). Due to its low frequency, infrasound can travel global distances with relatively low attenuation while higher frequency audible sound is usually dissipated at shorter ranges (Drob et al., 2003). Infrasonic waves may travel through the atmosphere between the Earth's surface and the thermosphere. The variability of wind and temperature with height determines the advection and refraction of infrasonic waves in the atmosphere (Gossard and Hooke, 1975).

15. SUBJECT TERMS

Dynamcis Azimuths

Microbaroms Topography

16. SECURITY CLASSIFICATION OF:			17. LIMITATION OF ABSTRACT	18. NUMBER OF PAGES	19a. NAME OF RESPONSIBLE PERSON
a. REPORT	b. ABSTRACT	c. THIS PAGE	SAR	70	19b. TELEPHONE NUMBER *(include area code)*
Unclassified	Unclassified	Unclassified			

ACKNOWLEDGMENTS

We would like to thank C. Hetzer for his analysis of microbarom signals, his help with the porting of WW3 into the Unix OS, and his help in processing the WW3 output files. Dr. S. Businger provided many helpful suggestions for the papers and research. We are profoundly grateful to H. Tolman, who introduced us to WW3, and to Paul Whittman, who provided valuable training and was essential to the implementation of WW3 into the Maui High Performance Computing Center. Many thanks also to Pierre Caron for his analysis of annual microbarom amplitude trends.

CONVERSION TABLE

Conversion Factors for U.S. Customary to metric (SI) units of measurement.

MULTIPLY → / ← TO GET	BY → / ← BY	TO GET → / ← DIVIDE
angstrom	1.000 000 x E -10	meters (m)
atmosphere (normal)	1.013 25 x E +2	kilo pascal (kPa)
bar	1.000 000 x E +2	kilo pascal (kPa)
barn	1.000 000 x E -28	meter^2 (m^2)
British thermal unit (thermochemical)	1.054 350 x E +3	joule (J)
calorie (thermochemical)	4.184 000	joule (J)
cal (thermochemical/cm^2)	4.184 000 x E -2	mega joule/m^2 (MJ/m^2)
curie	3.700 000 x E +1	*giga bacquerel (GBq)
degree (angle)	1.745 329 x E -2	radian (rad)
degree Fahrenheit	$t_k = (t°f + 459.67)/1.8$	degree kelvin (K)
electron volt	1.602 19 x E -19	joule (J)
erg	1.000 000 x E -7	joule (J)
erg/second	1.000 000 x E -7	watt (W)
foot	3.048 000 x E -1	meter (m)
foot-pound-force	1.355 818	joule (J)
gallon (U.S. liquid)	3.785 412 x E -3	meter^3 (m^3)
inch	2.540 000 x E -2	meter (m)
jerk	1.000 000 x E +9	joule (J)
joule/kilogram (J/kg) radiation dose absorbed	1.000 000	Gray (Gy)
kilotons	4.183	terajoules
kip (1000 lbf)	4.448 222 x E +3	newton (N)
kip/inch^2 (ksi)	6.894 757 x E +3	kilo pascal (kPa)
ktap	1.000 000 x E +2	newton-second/m^2 (N-s/m^2)
micron	1.000 000 x E -6	meter (m)
mil	2.540 000 x E -5	meter (m)
mile (international)	1.609 344 x E +3	meter (m)
ounce	2.834 952 x E -2	kilogram (kg)
pound-force (lbs avoirdupois)	4.448 222	newton (N)
pound-force inch	1.129 848 x E -1	newton-meter (N-m)
pound-force/inch	1.751 268 x E +2	newton/meter (N/m)
pound-force/foot^2	4.788 026 x E -2	kilo pascal (kPa)
pound-force/inch^2 (psi)	6.894 757	kilo pascal (kPa)
pound-mass (lbm avoirdupois)	4.535 924 x E -1	kilogram (kg)
pound-mass-foot^2 (moment of inertia)	4.214 011 x E -2	kilogram-meter^2 (kg-m^2)
pound-mass/foot^3	1.601 846 x E +1	kilogram-meter^3 (kg/m^3)
rad (radiation dose absorbed)	1.000 000 x E -2	**Gray (Gy)
roentgen	2.579 760 x E -4	coulomb/kilogram (C/kg)
shake	1.000 000 x E -8	second (s)
slug	1.459 390 x E +1	kilogram (kg)
torr (mm Hg, 0^0 C)	1.333 22 x E -1	kilo pascal (kPa)

*The bacquerel (Bq) is the SI unit of radioactivity; 1 Bq = 1 event/s.
**The Gray (GY) is the SI unit of absorbed radiation.

TABLE OF CONTENTS

Figures

Figures (Continued)

SECTION 1

INTRODUCTION

Naturally occurring sources of infrasound include (but are not limited to) severe weather, volcanoes, bolides, earthquakes, surf, mountain waves, and, the focus of this research, nonlinear ocean wave interactions. Man-made sources of infrasound also exist, such as airplane activity, military testing, rocket launches, and nuclear explosions (Bedard and Georges, 2000). Due to its low frequency, infrasound can travel global distances with relatively low attenuation while higher frequency audible sound is usually dissipated at shorter ranges (Drob et al., 2003). Infrasonic waves may travel through the atmosphere between the Earth's surface and the thermosphere. The variability of wind and temperature with height determines the advection and refraction of infrasonic waves in the atmosphere (Gossard and Hooke, 1975).

Infrasound station I59US, located at latitude 19.5915 N, longitude 155.8936 W (near Kailua-Kona, Hawaii) and operated by the University of Hawaii, is part of the global infrasound network of the IMS (Fig.1, Vivas-Veloso et al., 2002). Infrasound arrivals at I59US (Fig. 2) have been studied in detail to characterize the coherent background sound field (Garcés and Hetzer, 2001, 2002, 2003). A large portion of this ambient field is related to a pervasive signal known as microbaroms. Microbaroms are observed as a continuous atmospheric pressure oscillation with most of its energy between 0.1 and 0.5 Hz (Fig. 3). Microbaroms are detected at the I59US array as coherent bursts with durations of minutes, an RMS amplitude varying between ~10 mPa and ~100 mPa, and apparent phase speeds with roughly the speed of sound (~340 m/s) (Figs. 4,5). For infrasonic stations near the ocean, microbaroms comprise the low-wind noise floor. The microbarom peak is in the midst of the detection region for 1-kiloton nuclear explosion tests. Therefore, microbaroms can obscure a signal of interest.

The objectives of this project were to characterize microbarom signals observed in the Pacific and model the source processes that generate these signals, with the aim of determining infrasonic detection thresholds in the microbarom frequency range. We addressed these objectives by studying microbarom signals from selected case studies and associating the observed infrasonic amplitudes, signal arrival direction, and microbarom frequencies with the theoretical infrasonic source field generated by a prescribed ocean surface wave spectrum. In this report we describe how the amount of coherent and incoherent infrasonic energy in the microbarom frequency band is determined by a complex combination of lower and upper atmosphere winds and the proximity, dynamics, and intensity of open-ocean swells. This report summarizes the results of various meeting presentations, a Masters thesis (Willis, 2004), and three peer-reviewed papers (Willis et al., 2004, Garcés et al. 2004, Willis et al., submitted).

Microbaroms were first reported by Benioff and Gutenberg (1939) on an electromagnetic microbarograph at the Seismological Laboratory of the California Institute of Technology. At the time of their studies, there was no accepted hypothesis for microbaroms or their better-known seismic counterparts, microseisms. Longuet Higgins (1950) was the first to recognize and develop a theory for the excitation of microseisms through the interaction of standing ocean waves with the sea floor. Posmentier (1967) presented a theory similar to the approach of Longuet-Higgins that explained the source generation of microbaroms. Posmentier's theory

described a nonlinear pressure perturbation that arises at the air-sea interface when two ocean waves of opposite direction and similar frequencies meet. The corresponding acoustic wave was shown to gain properties of the interfering ocean wave train where acoustic amplitude is proportional to the product of the opposing ocean waves and frequency is twice that of the individual ocean waves. Arendt and Fritts (2000) extended this theory to an arbitrary spectrum of ocean surface waves. They found that the frequency-doubling nonlinear interactions of pairs of ocean waves traveling in nearly opposite directions produces propagating acoustic waves of an isotropic nature. All terrestrial ocean surface waves contain phase speeds and wavelengths much smaller than acoustic phase speeds and wavelengths. Thus, single ocean waves cannot couple sound into the atmosphere. However, sound can be coupled into the atmosphere when ocean waves interact nonlinearly and the sum of the horizontal wavenumbers of the ocean surface waves is nearly zero. This occurs only when an ocean wave spectrum contains components of nearly identical frequencies traveling in nearly opposite directions. Ocean waves propagating with identical frequencies in opposite directions are predicted to radiate sound vertically, leading to efficient ensonification into the ocean and seabed but ensuring that atmospheric sound never reaches the ground again. Thus, microseisms propagate through the ground as a result of vertical excitation through the ocean; microbaroms propagate to infrasonic stations after near horizontal propagation through the atmosphere (Tebulevich, 1995).

Studies by Saxer (1945, 1954), Daniels (1953, 1962), Donn and Posmentier (1967), Donn and Naini (1973) and Rind (1980) confirmed that the microbarom and microseism source is related to strong storms over the ocean and the resulting high seas. In addition to major weather systems (cold fronts, high and low pressure areas) and significant wave heights, Rind (1980) compared expected source locations of microbaroms and microseisms recorded at Palisades, New York with dominant wave period and mean propagation charts on a 5° grid provided by the Navy Fleet Numerical Weather Center. Since microbaroms theoretically contain frequencies twice those of the producing ocean waves, Rind attempted to correlate the period of the observed microbaroms with ocean wave half periods in the expected source regions. The mean propagation charts were used to correlate the expected source regions with areas that contained opposing wave trains. The methods of Rind (1980) were not effective in the case studies presented in this study. It should be mentioned that Rind discussed the error potential in correlating microbaroms with mean wave parameters on such a coarse grid instead of using any entire spectrum of waves. Advancements have been made in ocean wave modeling since 1980, which has made this present research possible.

Strong microbarom signals tend to arrive from regions of marine storminess because marine storms can produce regions of high amplitude ocean waves converging from opposite directions. Consider a symmetrical, westward moving tropical cyclone of the northern hemisphere (Fig. 6a). The surface low will contain similar fetch characteristics on all sides of the center, with the north side of a westward moving storm in the northern hemisphere generally containing the highest winds and seas. After the westward moving storm passes a given point, the swell spectrum at that point will eventually become confused with wave trains traveling in opposite directions that were created on both the northeast and southwest sides of the low center (Fig. 6b). Thus, the theoretical guidelines for microbarom productions will be met in the storm wake region, which is east of the center in the case of a westward moving tropical cyclone. In this study, we present case studies of eastward propagating middle latitude (extratropical) storms – in which the wake

region is normally to the west of the center. The wake region microbarom generation theory is discussed in Pnomaryov et al. (1998) and converging wave trains of opposite directions were also observed in the wake of Hurricane Bonnie in the Northwest Atlantic Ocean (Wright et al., 1998).

In the case of the eastward moving middle latitude storm, the south side of the storm will contain the strongest fetch lengths, durations, and intensities and thus higher wave heights and periods can be expected on to the south of the center. It is rare for an eastward moving storm to produce long wave periods of 13 seconds or more on the north side of the center unless the storm is a slow mover, large in diameter, and/or contains very high wind speeds. Furthermore, since long period swells exhibit higher group velocities than short period swells (group velocity of swells with 20 sec ~ 15 m/s ~ 29 knots; 5 sec ~ 3.75 m/s ~ 7 knots), the long period energy created ahead of a low center will often be dispersed before it has time to interact with any longer period energy that may be created behind the low center. This is especially true when the storm is moving slower than the group velocities of the long period ocean waves it produces. Steep, short period swells (< 8 seconds) often dissipate within a few wavelengths due to whitecapping and angular spreading effects. This can prevent opposing wave trains of short periods from interacting. On the other hand, opposing wave trains of medium periods (8-12 seconds) are very likely in wake of both middle latitude and tropical cyclones, and thus the infrasonic peak at 0.2 Hz is commonly observed (Fig. 3). If there are long period swells created on the north side of the center (in the case of an eastward moving storm), the amplitudes are normally small and thus the resulting infrasonic wave that results will also have small amplitude. Similarly, dissipating shorter period swells that may interact will also produce smaller amplitude infrasonic waves. This also helps explain the common infrasonic spectral peak at 0.2 Hz.

In this project the microbarom generation model of Arendt and Fritts (2000) and global wave spectra from the third-generation Wavewatch III (WW3) ocean wave model of Tolman (1999) are used to predict acoustic source pressure spectra. This will provide a global estimate of probable microbarom generation regions in the Pacific for the case studies presented (early January and late February, 2003). The source modeling results will also show the relationship between microbarom generation regions and marine storms and dominant ocean wave parameters (significant wave height, peak period, and mean propagation directions). Microbaroms observed at the I59US and other near-Pacific infrasound arrays will be used to confirm our modeling results. The observed and modeled microbaroms will be used together to help present a conceptual model of microbarom generation in the Pacific. This will help in the characterization of microbarom source regions observed at I59US during 2003. Finally, microbarom signals observed in Hawaii during 2003 are also compared to prevailing atmospheric winds to help further explain some of the seasonal and daily variability of the arrivals.

SECTION 2

DATA, METHODS, AND INSTRUMENTATION

The I59US infrasound array consists of four Chaparral-5 differential pressure microphones with a frequency range of 0.04 to 8 Hz. Three of the sensors are arranged as a triangle with a 2 km baseline, with the fourth sensor near the center of the triangle (Fig. 2). Sensor data are recorded at 20 samples per second by 24-bit digitizers and sent in real time via radio telemetry to the Infrasound Laboratory in Keahole Point on the west coast of Hawaii. The I59US station has very low ambient noise levels and is one of the most sensitive stations of the IMS because of its location in a dense tropical forest leeward of Hawaii's massive volcanoes. Porous hose filters are also used for wind noise reduction.

The Progressive Multi-Channel Correlation (PMCC) algorithm of Cansi et al. (1995) is the primary signal detection system used at I59US. PMCC uses the correlation between various groupings of three sensors, *i, j, k* to estimate the consistency of the lag-closure relation

$$r_{ijk} = \Delta t_{ij} + \Delta t_{jk} + \Delta t_{ki}, \qquad (1)$$

where Δt_{ij} is the time delay between the arrival of a signal at sensors *i* and *j* (Cansi and Klinger, 1997). For an ideal wavefront, this consistency is equal to zero. A microbarom detection is only registered if the consistency is below 0.5 sec within the 0.1-0.5 Hz passband (Garcés and Hetzer, 2002, 2003). The microbarom feature extraction process uses overlapping windows of data with a length of 90 sec and an overlap of 20 sec. In essence, PMCC is used to detect coherent infrasonic energy across the array, which allows the speed, arrival azimuth, and amplitude of the detected arrivals to be extracted. Microbarom arrival azimuth and amplitude is the main parameter we use to compare with storm and ocean wave characteristics as well as source modeling results. The arrival azimuth of an infrasound signal is obtained by determining time shifts that yield the highest cross-correlation between waveforms of the array elements. Signals with low consistency, as well as a steady azimuth and trace velocity, are referred to as coherent arrivals. Due to a 160 m sensor elevation difference (Fig. 2), the arrival azimuth and apparent horizontal phase velocity has to be corrected for energy incident at steep angles from the horizontal (D. Brown, personal communication, 2001). However, most microbaroms arrive near the horizontal, so no substantial correction is needed.

Infrasonic power spectral densities are used to distinguish peaks in the microbarom frequency range. The power spectral densities were computed using the modified periodogram method (Madisetti and Williams, 1998) with a 102.4 s Hanning window (2^{11} samples) and a 50% overlap. Power spectra include the combination of both coherent and non-coherent microbaroms at each frequency.

The WW3 ocean wave model (v1.18) is driven by NOGAPS 10 m surface winds and includes global ice concentration values and is used to produce realistic ocean wave spectra values on a global 1° grid. The wind and ice input files are provided by the Master Environmental Library Homepage (MEL) at http://mel.dmso.mil/. For both case studies discussed in this project, WW3

was initialized at least 6 days ahead of chosen events to produce an accurate background ocean wave field.

The WW3 model outputs wave energy densities, F, as a function of frequency, f, and propagation direction, θ. The wave energy densities can be integrated over angle and frequency to provide the total wave energy E,

$$E = \int_0^{2\pi} d\theta \int_0^{\infty} df F(f,\theta). \qquad (2)$$

The significant wave height is defined as

$$H_s = 4\sqrt{E}\,. \qquad (3)$$

WW3 outputs wave energy densities in 24 directional and 25 frequency bins to produce 600 values at each grid point. These wave spectra are then used to calculate acoustic source pressure by summing the products of directly opposing wave trains at each frequency. The following algorithm based on the Arendt and Fritts (2000) model was used to predict acoustic source pressure fields on a global 1° grid,

$$P_k^0 = \frac{\rho c g^2}{4\omega_m}\left[\int_0^{2\pi}\sqrt{F(k_x,k_y)F(-k_x,-k_y)}\,d\theta\right] = \frac{\rho c g^2}{4\omega_m} Q_m^0 \qquad (4)$$

$$Q_m^0 = \int_0^{2\pi}\sqrt{F(k_x,k_y)F(-k_x,-k_y)}\,d\theta = 2\int_0^{\pi}\sqrt{F(f,\theta F(f,\theta+\pi))}\,d\theta \qquad (5)$$

where P_k (Pa·m^3) is the acoustic source pressure wavenumber spectrum, ω_m is the microbarom frequency which is assumed to be twice that of the ocean surface waves, ρ, c, and g are assumed to be 1 kg·m^{-3}, 340 m·s^{-2} and 9.81 m·s^{-2}, respectively. Q_m contains the product of WW3 produced wave energy densities traveling in opposite directions with frequency held constant, integrated over all 24 directional bins. A detailed derivation of this algorithm is given in Garcés et al. (2003) and Appendix A.

WW3 is considered by academia, military, and ocean enthusiasts alike to be one of the best ocean wave models of its kind to date. Global WW3 output validates well when compared to both buoy and satellite altimeter observations (Tolman, 2002). Tolman (2002) also showed the superiority the WW3 model has to its predecessor, the Wave Action Model (WAM). The WAM model was shown to perform poorly in large ocean basins (i.e. the Pacific) due to wave generation and propagation errors, while WW3 has made improvements in these schemes (Rogers and O'Reilly, 2002).

Observational and source modeling results are first shown for January 4, 2003 at which time an intense (sub 952mb) mid latitude cyclone was moving eastward just north of the Hawaiian Islands, along with 6 other surface lows scattered throughout the Pacific Basin. The second case

study is from February 22, 2003 when the North Pacific was also very active with storm and high wave activity. Both of these case studies were chosen primarily because of the strength and coherence of the microbarom observations during the events. Microbarom arrival azimuths from 7 other infrasound stations were obtained from the February 22 event, which allowed for the triangulation of the microbarom source region. Five of these stations are part of the IMS: IS34 (Mongolia, China), IS53 (Fairbanks, Alaska), IS57 (Pinion Flat, California), IS10 (Manitoba, Canada), and the Hawaii IS59 array. Non-IMS sites PDIAR (Pinedale, Wyoming) and NVIAR (Mina, Nevada) also recorded microbaroms from the North Pacific on February 22.

Surface pressure charts were generated using data supplied by the NCEP/NCAR Reanalysis project available in 6 hourly intervals at a resolution of 2.5° (web site at www.cdc.noaa.gov/). The NCEP/NCAR data set provides a good opportunity to examine the synoptic scale evolution of storm systems. Surface weather and wave charts are compared to microbarom observations and source modeling results to distinguish a relationship between infrasonic source locations and marine storm tracks.

Since meteorology determines how sound travels, this research also relates seasonal and daily microbarom arrivals to predominant wind directions from the troposphere to the mesosphere (Chapter 4). In order to produce atmospheric specifications for infrasonic propagation studies, the Naval Research Laboratory (NRL) Ground to Space (G2S) model (Drob et al., 2003) was run to produce a self-consistent dataset extending from January 1, 2003 to March 29, 2004. Global spectral coefficients of wind, temperature, and density were produced at 6-hour time intervals. These coefficients have a triangularly truncated spectral order of 72 (T-72) resulting in an effective output resolution of approximately 2.25 degrees. The G2S winds from the Earth's surface to 10 mb (0 to 35 km) are based on analysis output from the 1x1 degree global aviation model (AVN) from the NOAA National Center for Environmental Prediction (NCEP). From 1 to .4 mb (20 to 55 km) the G2S winds are based on the 1.0x1.5 global assimilative analysis from the NASA Goddard Space Flight Center, Global Modeling and Assimilation Office (GSFC-GMAO). The upper atmospheric conditions (50-170 km) are specified by the HWM/MSIS models.

SECTION 3

MICROBAROM OBSERVATIONS AND SOURCE MODELING RESULTS FROM TWO CASE STUDIES DURING THE WINTER OF 2003

The I59US station gets bombarded with coherent microbarom arrivals from 250-360° during the Boreal Winter, which is where the strongest storms and highest seas tend to be located from around November through March. Fewer arrivals come from northeast azimuths during the winter despite the common presence of strong storms and high seas northeast of the Hawaii array. This appears to be a result of topographic shadowing and advection of the predominant winds (discussed in further detail in Chapter 4). It is not uncommon for the daily variability of arrival azimuth to exhibit a clockwise rotation as storm systems travel from west to east in the North Pacific. Sometimes however, microbarom arrivals do not appear to follow storm systems. The aim of this chapter is to compare microbarom observations to source modeling results, surface weather charts, and dominant wave parameters to better characterize microbarom source regions.

3.1 MICROBAROM OBSERVATIONS FROM EARLY JANUARY 2003

Microbarom arrivals from Jan. 1-3, 2003 concentrated between 270-330° (Fig. 7) correspond to surface low pressure areas and high wave activity in the region during that time. Of particular interest are arrivals from Jan. 4-6, 2003. Peak microbarom signals on the 4th are from northwest azimuths. The arrival peak then rotates clockwise through the 5th when several arrivals from the northeast are evident. Coherent energy from both west and northeast directions are recorded on the 6th. A middle latitude cyclone with central pressure < 952 mb was located just northwest of Hawaii on the 4th and then moved northeast of I59US on the 5th (Fig. 8), similar to the directions the microbaroms were coming from. This storm system produced massive NW swells along exposed Hawaiian Island shores on Jan. 5-6, 2003, with observed breaking wave heights > 12 m closing out Waimea Bay.

Seven surface low pressure centers can be seen in the Pacific Ocean and its nearby waters on Jan. 4, 2003 at 18Z (Fig. 9). Each of these has an associated peak in significant wave height (Fig. 10) that is located where pressure gradients are strongest. Four of these lows are in the southern hemisphere but little to no coherent microbaroms from southerly directions was recorded during this time frame. These observations suggest that the microbaroms from early January 2003 are coming from North Pacific storm systems and/or their associated regions of converging high seas. Comparison of microbarom arrivals at I59US during this time to dominant wave period and direction charts (Fig. 11) yielded no clear relationship. However, it is nearly impossible to pinpoint an exact source location region from the arrival azimuth data from the I59US array alone. Data from other arrays was investigated, but no similar source region was noted as signals from storms adjacent to those stations dominated.

The infrasonic power spectrum on Jan. 4, 2003 18Z (Fig. 3) shows a peak of 0.1 Pa^2/Hz near 0.2 Hz. A smaller peak of .01 Pa^2/Hz is seen near .135 Hz. A minimum of less than .001 Pa^2/Hz is evident near 0.1 Hz. The microbarom peak at 0.2 Hz is typical year round at I59US. A

microbarom containing a frequency of 0.2 Hz would theoretically originate from two swell trains containing periods of 10 seconds (0.1 Hz) traveling in nearly equal but opposite directions. Of particular interest is the spectral increase in energy from 0.1 to 0.2 Hz from Jan. 4 (Fig. 3) to Jan. 6 (Fig. 12). This increase corresponds to an increase in interactions of ocean waves containing longer periods (10 to 20 sec).

3.2 SOURCE MODELING RESULTS FROM JANUARY 4-6, 2003

Six out of seven surface low pressure centers in or near the Pacific Ocean on 01/04/18Z exhibit a peak in acoustic source pressure at 0.197 Hz just west or southwest of the center of circulation (Fig. 13). Lows with a peak in acoustic pressure to the southwest of the center were propagating to the northeast while lows with a peak to the west of the center were propagating more towards the east. The exception is the surface low centered in the extreme NW Pacific (just north of Hokkaido, Japan) where a maximum in acoustic pressure is noted to the south of the low center. This storm was propagating just east of due north. The acoustic source pressure peak seemingly associated with this low also appears to be much larger and broader than the other peaks. Several other high source pressure regions 0.197 Hz are noted throughout the Pacific at this time in regions near anticyclones and weak surface pressure gradients.

Another interesting finding is the minima in source pressure at 0.197 Hz found in the immediate vicinity and just southwest of the strong cyclone just NNW of the Hawaiian Islands. The acoustic peak at 0.197 Hz is further upstream of the center in this storm than the others. Acoustic source pressure calculations at lower frequencies show a peak closer to this low center (Fig. 14). The microbarom source at 0.122 Hz shows a maximum just southwest of the center of the storm. Microbaroms containing frequencies of 0.122 Hz correspond to opposing ocean waves colliding with frequency .061 Hz (16.7 second periods). These longer wave periods are a direct relationship to the strong storm's high winds and long fetch lengths. Although the observed microbarom spectral peak is normally ~ 0.2 Hz, microbaroms of lower frequencies can be generated in cases such as this and thus must be considered.

Modeled infrasonic source pressures with frequency 0.135 Hz from Jan. 4 00Z to Jan 6 00Z were also inspected (Fig. 15), due to the observed increase in infrasonic power at this frequency during the time. Of the 3 lows present in the North Pacific, each exhibited a wake region peak in modeled acoustic pressure at 0.135 Hz. However, there were also other high acoustic source pressure regions noted in the North Pacific during this time (some >1000 km from storm location).

As the strong storm just northwest of the Hawaiian Islands (Labeled "L_2" in Fig. 15) intensified, increased in diameter, and pushed towards the ENE/NE, the peak in acoustic pressure in its wake (at 0.135 Hz) also increased in amplitude and diameter and moved ENE/NE. The microbarom signals observed at I59US during this time show a similar trend. However, not all of the arrivals during this time match up with the wake region of the strong low L_2. There are also arrivals coming from W and NW directions where WW3 also predicted high acoustic source pressure regions after low L_2 moved N and NE of I59US.

The clockwise rotation of the observed arrival azimuths from Jan. 4-6 track well with the modeled microbarom sources at 0.135 Hz. The other arrivals during this early January case not associated with storm wake regions validate well to the low frequency source modeling results as well. There are also similarities in the modeled sources at 0.2 Hz with the observations, but overall the observations tend to track better with the lower frequency sources in this case. We postulate that, for this case study, the low-frequency microbarom source dominated amongst all possible arrivals because of its high energy, large spatial extent, proximity to the island, and longer period. For these energetic swells, the prevailing winds may play a secondary role to the source strength and arrivals may reach the station from any azimuth.

3.3 MICROBAROM OBSERVATIONS FROM LATE FEBRUARY 2003

In contrast to the early January event, microbarom arrival azimuth at I59US from February 19-25, 2003 shows little directional variation. Most of the energy between 0.1 and 0.5 Hz during this period came from 310° +/- 10° (Fig. 16). There were several eastward propagating surface lows in the North Pacific during this time frame. This pattern is unlike the January 3-5 pattern, which showed a clear clockwise rotation in the arrival azimuths as a strong storm system moved east. The continuous signal from ~310° (instead of arrivals following storm systems) during this time suggests that microbarom source generation regions are not simply related to surface low (Fig. 17) or highest ocean wave (Fig. 18) location. No clear relationship was noted between arrival azimuth and peak wave period or directions (Fig. 19) either.

On February 22, 2003 low frequency energy below 0.6 Hz that originated from a region in the North Pacific was recorded on 8 different infrasound stations throughout the Northern Hemisphere and lasted for several hours. This exceptional microbarom burst was much stronger than normal microbarom events (Fig. 5) and thus was recorded by eight infrasound arrays: IS10, Canada, IS34, Mongolia, IS53, Alaska, IS56, Washington, IS57, California, IS59, Hawaii, PDIAR, Wyoming, and NVIAR, Nevada. Near the peak of this infrasound event at 00Z on the 22nd, three surface low pressure systems were evident in the North Pacific. The first was an intense cyclone just east of Japan, centered near 40N, 168E with a minimum central pressure below 960mb. A second, moderately strong and symmetrical surface low (988mb) was located near 45N, 155W while a third but much weaker closed low was centered just north of the western Aleutian Islands near 55N, 172W. The first two cyclones were propagating towards the ENE while the 3rd was moving slowly and erratically.

The microbarom back azimuths extended along great circle routes from 7 of the 8 infrasonic arrays during the peak of this event intersect in a confined region between 25-32N and 168-170W, which is not a region where a surface low or peak in significant wave height is noted. The only station whose microbarom back azimuth did not intersect through this region was IS10. IS10's great circle intersects with IS53 just south of the central Aleutian Islands, with IS34 just west-southwest of the first, strong low and with IS59 near 32N, 145E. The observations of this event are discussed in detail in Bhattacharyya et al. (2003).

3.4 SOURCE MODELING RESULTS FROM FEBRUARY 22, 2003 00Z

Highest predicted acoustic source pressure values in the Pacific Basin from 00Z on February 22 are evident in the Northwest Pacific basin. Much of the modeled high acoustic source pressures appear to be located in or near the wake regions of the two surface lows that were propagating east-northeast (Fig. 20). However, some of the higher acoustic pressure values are evident between the two surface lows. This is associated with swells with a westerly component produced by the westernmost storm interacting with swells with an easterly component produced by the easternmost storm. Nearly all microbarom energy received at I59US during this time frame came from the direction of these modeled peaks in acoustic source pressure. However, it is difficult to tell exactly which region of converging ocean waves the infrasound is coming from since the modeled peaks in acoustic pressure are of similar azimuth from the I59US array.

Other maxima in modeled acoustic source pressure are noted besides the major North Pacific peaks: a broad maxima east of Hawaii extending north of the Equator through 50N between longitudes 120 and 150W, a peak just west of Peru, and several other Pacific Basin high pressure values scattered throughout the southern hemisphere middle to higher latitudes. Several of these are in regions of a dominating anticyclone or weak pressure gradients.

The opposing wave train theory verifies well when we compare the infrasound observed from the 8 stations during this event with the WW3 produced source values. The great circle paths associated with the arrival azimuths at these stations do not intersect over a peak in significant wave height (Fig. 18) or near the center of the major surface lows in the region (Fig. 17). Instead, the great circles intersect in regions of the WW3 produced high acoustic source pressures (Fig. 21).

SECTION 4

COHERENT MICROBAROM ARRIVALS AT I59US DURING 2003 AND THEIR RELATIONSHIP WITH STORMS, TOPOGRAPHY, AND PREVAILING ATMOSPHERIC WINDS

Microbarom arrival azimuths at the I59US site during 2002 and 2003 show an annual cycle (Fig. 22). During the months from June through September microbarom arrivals generally come from east (55-130°) or south (160-220°) directions. The concentration of east arrivals is much stronger than the south arrivals during this time. The months of October through March show an abundance of arrivals from 230-360° with a peak from northwesterly directions. The winter arrivals also have higher amplitudes than other seasons. Arrivals during April, May, late September and early October appear to arrive from a variety of different azimuths with no distinct peak noted.

Annual arrivals clearly correspond to dominant storm activity in the Pacific Basin but are also affected by topographic shadowing and zonal and meridional winds throughout the atmosphere. Acoustic shadowing by the Mauna Loa and Hualalai volcanoes may explain the few arrivals from ~ 150° and 25°, respectively. Microbarom arrival azimuth also shows a fairly strong relationship with the dominant wind directions in the troposphere, stratosphere, and mesosphere (Fig. 23). Some of the seasonal trends in the microbarom observations can be explained by the winds in the stratosphere and lower mesosphere (50-70 km), while some of the daily variability can be explained by the tropospheric and lower stratospheric winds (10-20 km). The wintertime W and NW arrivals relate well to the predominant winds at these levels in the atmosphere, as do the summer time arrivals from the east. However, the summer time arrivals from the south do not correspond well with the winds. Figure 24 shows a close up of Figure 23 for the months of January and February of 2003. These are some of the most active swell months for the Hawaiian Islands. Some of the microbarom arrival azimuths in January and February track the tropospheric winds very well, corresponding to energy that would be refracted back to the ground at the 10-20km height in the atmosphere, where there is very little attenuation. Likewise, energy ducted between the stratopause and the ground would suffer very little attenuation and thereby retain relatively large amplitude. An interesting feature is that the 10-20km wind directions above Hawaii during the early January and late February cases presented in Chapter 3 show little to no relationship with the microbaroms arrival azimuth at IS59. The marine storms responsible for these microbarom events produced high open ocean wave heights over a wide spectrum of frequencies between 0.05 and 0.1 Hz, and thus produced high microbarom source amplitudes between 0.1 and 0.2 Hz. High source amplitudes, coupled with lower attenuation and larger correlation length at lower frequencies, would permit long-range propagation of this energy over large distances and preferential detection by an array. As in the January 4-6 case study, microbarom signals may overcome the atmospheric conditions along the propagation path if the source amplitude is sufficiently strong and contains a lower frequency (< 0.2 Hz).

A total of 21459 coherent microbarom arrivals reached I59US in 2003 (Fig. 25). 9334 of these arrivals (43%), the vast majority, came from 270-315°. The second highest 45-degree directional bin, 225-270°, contained 4211 (19.6%) microbarom arrivals during 2003. 2606 arrivals (12%)

came from 45-90°, 1605 (7.5%) from 315-360°, 1599 (7.5%) from 180-225°, 1168 (5.4%) from 0-45°, 549 from 90-135°, while only 377 arrivals came from azimuths 135-180°.

During the first quarter of 2003 (containing months December 2002, January and February 2003), 98% of the microbarom arrivals came from azimuths 225-360° (Fig. 26). The second quarter of 2003 (March, April, May) shows a similar directional dependence with 81% of the arrivals coming from 225-360° (Fig. 27). However, stronger signatures from 0-90° (13%) and 180-225° (4%) were evident in Quarter 2 than in Quarter 1.

A very different pattern of microbarom arrival azimuth was observed during the boreal summer months of Quarter 3 (Fig. 28). 70% of the arrivals during June, July, and August came from 0-135° while 26% came from 135-225°. Arrivals at I59US during the fall months of Quarter 4 (Fig. 29) show a very similar pattern to the springtime Quarter 2 arrivals – with 72% coming from 225-360°, 13% from 0-90°, and 10% from 180-225°.

The observed arrivals during 2003 suggest a relationship between microbarom arrival azimuth, dominant storm activity in the Pacific Basin, and tropospheric, stratospheric, and mesospheric winds above Hawaii. Boreal wintertime arrivals at I59US come from west and northwest directions, while summer arrivals come primarily from east and south azimuths. Arrivals during the shoulder seasons are more evenly distributed around the compass. Microbaroms observed at I59US come primarily from regions where storm and wave activity are the strongest throughout the year, as suggested in Chapter 3, but are also strongly affected by the prevailing winds in the troposphere, stratosphere, and mesosphere. Reflections from coastlines may produce a portion of the arrivals at I59US.

SECTION 5

SUMMARY, CONCLUSIONS, AND DISCUSSION

5.1 SUMMARY AND CONCLUSIONS

In this research, the microbarom generation theory of Arendt and Fritts (2000) is used with ocean wave spectra provided by the WW3 model to predict acoustic source pressure fields generated by opposing wave trains in the open ocean. Standing ocean surface waves are created when opposing wave trains of similar frequencies and near opposite directions meet. This interaction generates a nonlinear pressure perturbation at the air-sea interface that travels as an infrasonic wave through the atmosphere. In this study, two detailed case studies with modeling results from the winter season of 2003 are documented. In addition, all of the coherent microbarom arrivals at the I59US site during 2003 are analyzed and described. The objectives of this research are to identify and characterize microbarom source regions in the Pacific basin and to show their relationship with storm and ocean wave activity. The following conclusions are drawn from a careful comparison of microbarom observations with simulated acoustic source pressures derived from the output of the Wavewatch III model:

1) The results from two detailed case studies show that observed microbarom arrival azimuths coincide well with strong infrasonic source regions predicted by the WW3 model, suggesting that the theoretical basis for the open ocean generation of microbaroms is substantially correct. Mean wave parameters such as significant wave height, peak period, and mean propagation direction are not effective in determining microbarom source regions. Conversely, WW3 is only able to produce an accurate depiction of microbarom source regions generated by open ocean wave interactions when the entire spectrum is used.
2) Microbaroms are generated wherever ocean surface wave trains with opposite propagation directions and similar frequencies interact. The strongest microbaroms are often generated in the wake regions of marine storms, where the amplitude of the opposing wave trains is greatest. In the two case studies, every propagating surface low exhibits a modeled wake-region peak in source pressure. However, high amplitude opposing wave trains can occur almost anywhere in the winter hemisphere where multiple mid-latitude storms may be evident. Thus, high acoustic source pressure regions are often prevalent at a distance from the wave producing winds.
3) Opposing wave trains and thus microbarom source regions are very common and can occur nearly anywhere in the ocean at any given time. All source regions may produce coherent or non-coherent arrivals at an array site but the strongest and most coherent signals will be determined by 1) amplitude and frequency of opposing wave trains, 2) proximity of high acoustic source regions to array site, 3) mesospheric, stratospheric and tropospheric winds, 4) thermospheric refraction, and 5) topographic shadowing.
4) The majority of wintertime microbarom arrivals at I59US come from west and northwest directions, while summer arrivals come primarily from east and south azimuths. Arrivals during the shoulder seasons are more evenly distributed around the compass. This annual cycle is the result of the variation of the most energetic storm/swell source locations during the year along with the prevailing wind directions between 10-20 km and 50-70 km.

5) Infrasound stations receive coherent arrivals from the closest and strongest source whose propagation path is favored by the atmospheric conditions, therefore weaker signals will be masked, including those generated in wake of distant or weaker storms.

5.2 DISCUSSION

Past research and this research show that microbaroms often arrive from regions of marine storm regions and the associated high seas. This study presents a relationship between marine storms/high seas with microbarom arrivals but it is not a direct relationship. The proposed generation theory for microbaroms does not appear to be related to any atmospheric phenomena associated with the storm itself, but rather to the ocean waves it creates.

Microbaroms observed at I59US from January 3-6, 2003 appeared to come from a region near the center of a strong surface low and the associated peak in significant wave height as the storm propagated west to east. In reality, these arrivals that appeared to be coming from the storm center were likely originating just in the wake of the center, where the swell spectrum was confused with multidirectional components created ahead of and behind the surface low center (Fig. 30). However, it is nearly impossible to tell the exact source locations of the microbaroms based on arrival azimuth data from one infrasound array only. Data from a network of observing stations during the February 22 REB event confirmed that microbaroms are not necessarily generated in regions of high significant wave height or where a marine storm is located. All of the back azimuths from this event converged over regions of high acoustic pressure (computed by output from the WW3 model), which were not collocated with peaks in significant wave height or surface low location.

Source modeling results from both of the case studies exhibit peaks in acoustic pressure in the wake regions of every moving marine storm in the Pacific Basin. The microbarom relationship with wake regions is clear in the early January case since the microbaroms rotate clockwise with time. However, the arrivals at I59US from February 19-25 show little directional variation dependency associated with moving storm systems. The dominant arrival azimuth for microbaroms at I59US during this time was near 310°. During the Northern Hemisphere winter, the seas in the northwest Pacific Ocean are often fully developed due to the persistence of strong mid-latitude cyclones. The storm track during this portion of February likely produced a broad, nearly continuous region of high seas converging in a region ~310° from I59US that was producing stronger microbarom signals than any of the other generation regions in the Pacific.

When multiple propagating surface lows are evident in the ocean simultaneously, each storm may generate a strong region of microbaroms in its wake or there may be strong source regions between the storms. Infrasound sites detect coherent signals from the closest and strongest source whose propagation path is favored by the atmospheric conditions; therefore, weaker and/or more distant sources are masked. Data from a network of infrasound sites are needed to determine an exact microbarom source region. The network of operational infrasound stations near the North Pacific may allow microbaroms generated in the wake of or between strong storm systems to be traced back to their source region.

The fact that infrasound sites detect signals from the closest and strongest sources favored by the atmosphere explains several of the other modeled peaks in acoustic source pressure. The results from both February 22 and January 4 showed source peaks in the wake regions of southern hemisphere low pressure systems but little to no coherent microbaroms were recorded from the south during either of the case studies. Arrivals from southern hemisphere sources are less obvious because of the effect of atmospheric conditions and attenuation along lengthy propagation paths. Source modeling also showed several weaker peaks scattered through the Pacific under regions of high atmospheric pressure at the surface and in weak wind regions. At any given time in the middle of the ocean there may be numerous multidirectional and multi-period swell events, typically more than three but less than 20, passing through a given point – regardless of storm or dominant swell activity in the vicinity. This is illustrated well by comparing the frequency and directional ocean wave spectrum at a Central Pacific location (Fig. 31) with surface pressure (Fig. 9) and significant wave heights (Fig. 10). The wave spectrum at this location (0° N, 153.88° W) shows five different swell peaks arriving simultaneously, but weak surface weather patterns are dominating and no peak in significant wave height is noted. Opposing wave trains and microbarom generation are therefore common at considerable distances from regions of strong wave generation. In particular, both case studies exhibit a broad peak in modeled source pressure in a region east of the Hawaiian Islands north of the Equator through 50N between longitudes 120 and 150W. The peaks here seem to be of only slightly weaker magnitudes to those in the wake regions of the strong North Pacific storms. This is arguably a result of the scale (log) used to plot these tiny pressure waves that rarely exceed a few mPa. The microbaroms generated in this region are expected to be weaker than those in the Northwest Pacific, and thus were not recorded on a coherent basis, but may indeed arrive as incoherent signals. There are also two other factors that could have prevented their coherent arrival at I59US: the strong deep layer westerly flow and the shadowing from Mauna Kea, Mauna Loa, and Hualalai volcanoes. Weak source regions may often produce incoherent energy at an array site, but the strongest and closest microbarom source region will generally determine the coherent signals.

Coherent microbarom signals at Kona generally come from south or east directions during the boreal summer. It is suggested that the arrivals from the south in the boreal summer originate from opposing wave trains in the wake regions of eastward propagating extratropical storms in the middle latitudes of the southern hemisphere. It is suggested that the east arrivals originate from 1) tropical weather in the East Pacific and 2) trade wind swells reflected from the Hawaiian Island chain. Incident trade wind swells are normally from 50-90° (NE to E) and are very common on the windward beaches of the Hawaiian Islands due to a persistent subtropical anticyclone that dominates the Pacific waters to the northeast much of the year. Sanderson (1993) discussed that northeast to east winds (trades) are present in the Hawaiian Islands from 85 to 95% of the time in summer, and from 50 to 80% of the time in the winter. Reflected swells by a land mass are a function of the incident amplitude and period, along with the steepness and permeability of the coastline (Shore Protection Manual, 1973). The Windward Shores of Hawaii have an abundance of rocky, steep coastline so microbarom generation by reflections is likely (Fig. 32). Trade wind swells typically range in period from 8-10 seconds. An incident trade swell from the east with period of 10 seconds interacting with a reflected trade swell from the west would produce an infrasonic wave with frequency 0.2 Hz as predicted by the frequency doubling nonlinear interactions theory (Arendt and Fritts, 2000). Therefore, microbarom

generation by reflections may explain part of the common infrasonic spectral peak at 0.2 Hz observed at I59US throughout the year, especially during summer months.

Occasionally, infrasonic power spectra observed at I59US exhibit split peaks within the microbarom threshold (Fig. 33). The peak at ~ 0.2 Hz is quasi-permanent but an increase in lower frequency energy sometimes leads to a bifurcation in this peak. This may be the result of two strong regions of opposing wave trains interacting. For example, microbaroms generated by ~10 s trade wind swell reflection may be occurring simultaneously with microbaroms being generated by longer wave period swells associated with tropical cyclones in the East Pacific. The trade swell reflection would lead to a peak at 0.2 Hz while the tropical cyclones produce a split peak at lower frequencies. This situation can also occur in the winter when multiple mid-latitude cyclones in the North Pacific produce numerous regions of converging wave trains of varying periods (as shown in the early January case). Thus it is possible to explain the structure of ocean-related infrasound spectra observed in Hawaii by attributing (1) a broad 2-5 Hz energy peak to breaking ocean waves (surf) in the littoral zone, (2) 0.2 Hz energy to the predominant 10 s swell energy and (3) 0.1-0.2 Hz energy to 12-20 s period swells associated with powerful storms. The surf peak depends on the swell energy arriving near the array site, and in Hawaii surf sound appears to be propagated in the boundary layer and the troposphere. The coherent component of the main microbarom peak at 0.2 Hz depends on the prevailing winds and the amount of swell energy in the ocean. However, the energy of the main microbarom peak is the sum of coherent and incoherent components, and the amplitude of this peak may be related to the diurnal tides in the upper atmosphere (Rind, 1978). If atmospheric winds do not support tropospheric or stratospheric waveguides, a low trace velocity could correspond to refraction in the mesosphere and lower thermosphere. Coherent microbaroms in the ~0.12-0.2 frequency range may arrive from any direction where energetic long-period swells are interacting, and under certain circumstances may also be used to study the mesosphere and lower thermosphere (Garcés et al., 2002). Returns from the upper atmosphere would explain southerly arrivals associated with the powerful southern hemisphere swells during the boreal summer.

Microbarom arrivals were shown to be concentrated from north and west directions during the Boreal winter. Arrivals with a northerly component are hypothesized to originate from non-linear interactions of ocean swells generated by eastward moving extratropical storms in the mid-latitudes of the North Pacific. Arrivals from west or west-southwest directions in the boreal winter are likely from Western Pacific tropical cyclones, including those that recurve during extratropical transition (when tropical cyclones lose their warm core characteristics while transitioning into a cold core mid-latitude cyclone). The west arrivals during the winter could also be generated by maturing cold core weather systems as well. Swell convergence associated with the Intertropical Convergence Zone (ITCZ) can also produce microbarom arrivals at I59US throughout the year from southeast, south, or southwest directions. Arrivals during fall and spring months were shown to come from a variety of directions with no distinct trend noted, due to the randomness of storm systems in the Pacific Basin during shoulder seasons.

The varying atmospheric conditions throughout the year are also expected to have a great influence on the microbarom arrivals. Microbaroms are believed to travel through a great extent of the atmosphere instead of directly on the horizontal (Gossard and Hooke, 1975). This leaves the sound waves vulnerable to numerous influences from the varying atmospheric conditions

during the year. The change in temperature with height will affect the propagation of the sound waves, as the phase speed of sound is proportional to the square root of the temperature. I59US may be more inclined to receive microbaroms from the west and northwest in the winter and from the east and northeast during summer because of the advection of the sound waves by the mean flow as show in Chapter 4. Figures 23 and 24 suggest that seasonal trends in microbarom arrival azimuth are associated with stratospheric wind directions while daily variability in arrivals may be explained by upper tropospheric wind patterns. In addition, substantial diurnal variability may be introduced by diurnal boundary layer fluctuations (Fig. 34). However, not all of the arrivals can be explained solely by wind direction. The strong microbarom signals observed at I59US during the case studies presented, for instance, show little correlation with the winds over Hawaii. This suggests that a strong, close microbarom source region may produce coherent energy at an array site regardless of the atmospheric conditions in the region. The issue of atmospheric wind effects on annual microbarom arrivals at I59US is discussed in detail in Garcés et al. (2004).

5.3 CONCLUDING REMARKS AND FUTURE WORK

Although in general the continuous microbarom noise is uncorrelated at I59US, distinct microbarom packets can be detected in Hawaii. When designing an array it may be useful to retain the coherence of microbaroms, as then it is possible to remove this contribution from a signal of interest.

This research computed acoustic source pressures calculated by colliding ocean waves given by the global 1° WW3 model. There will certainly be subgrid scale regions that contain opposing wave trains and thus microbarom generation regions. The next step of this project will involve transporting the WW3 model to the Maui High Performance Computing Center (MHPCC) to refine the resolution of both the wave and microbarom source modeling. A high resolution bathymetry file and shallow water, near shore ocean physics would need to be incorporated into the ocean modeling to show the microbarom source regions associated with reflections from a coastline.

Producing an accurate model of the microbarom source is only the first step in a very complex problem. The modeled source pressures need to be propagated across the globe with atmospheric specifications (wind, temperature, pressure, and density), topography, attenuation, and propagation time taken into account in order to define microbarom noise at an array site. Global-scale infrasound propagation modeling is beyond the scope of this report.

The results presented in this document show there is potential for using microbaroms to track ocean wave activity. Buoy and ship observations are scarce while wave parameters from satellite interpolations are not continuous because they are obtained through satellites on polar orbits. Incidentally, infrasonic energy in the 2-5 Hz range associated with surf breaking has been shown to be closely correlated to significant wave heights recorded by a nearby buoy. This also is beyond the scope of this paper but is discussed in Garcés et al (2003). Microbaroms contain information about the wave periods and amplitudes of the generating open ocean waves. Wave period is often a parameter that goes overlooked in operational forecasting, but in fact is a crucial component to the prediction of breaking wave heights.

SECTION 6

REFERENCES

Arendt, S., and D. Fritts, 2000: Acoustic radiation by ocean surface waves. *J. Fluid Mech.*, **415**, 1-21. (UNCLASSIFIED)

Bedard, A. and T.M. Georges, 2000: Atmospheric Infrasound. *Physics Today*, **53(3)**, 32-37. (UNCLASSIFIED)

Bhattacharyya, J., C. Hetzer, M. Garcés, and V. Oancea, 2003: Description and Analysis of Infrasound Signals Recorded from the North Pacific Event of February 22, 2003, presented at the Infrasound Technology Workshop, La Jolla, California, October 27-30. (UNCLASSIFIED)

Benioff, H. and B. Gutenberg, 1939: Waves and currents recorded by electromagnetic barographs. *Bull. Am. Met. Soc.*, **20**, 421. (UNCLASSIFIED)

Cansi, Y., 1995: An automatic seismic event processing for detection and location: The P.M.C.C. method. *Geophys. Res. Lett.*, **22**, 1021-1024. (UNCLASSIFIED)

Cansi, Y., and Y. Klinger, 1997: An automated data processing method for mini-arrays.*Newsletter of the European-Mediterranean Seismological Center*, **11**, 2-4. (UNCLASSIFIED)

CTBTO, cited 2004: History of the Comprehensive Nuclear-Test-Ban-Treaty (CTBT). [Available Online at http://www.ctbto.org]. (UNCLASSIFIED)

Daniels, F. B., 1952: Acoustical energy generated by the ocean waves. *J. Acoust. Soc. Am.*, **24**, 83. (UNCLASSIFIED)

Daniels, F. B., 1962: Generation of infrasound by ocean waves. *J. Acoust. Soc. Am.*, **34**, 352-353. (UNCLASSIFIED)

Donn, W. L. and E. S. Posmentier, 1967: Infrasonic waves from the marine storm of April 7, 1966. *J. Geophys. Res.*, **72,** 2053-2061. (UNCLASSIFIED)

Donn, W. L. and B. Naini, 1973: Sea wave origin of microbaroms and microseisms. *J. Geophys. Res.*, **78**, 4482-4488. (UNCLASSIFIED)

Drob, D. P., J. M. Picone, and M. Garcés, 2003: Global morphology of infrasound propagation. *J. Geophys. Res.*, **108(D21)**, 4680. (UNCLASSIFIED)

Garcés, M, and C. Hetzer, 2001: *Infrasonic signals detected by the Kona array, Hawaii.* 23rd Annual DTRA/NNSA Seismic Research Review, Jackson Hole, 1-5 October 2001. (UNCLASSIFIED)

Garcés, M. and C. Hetzer, 2002: Evaluation of Infrasonic Detection Algorithms. 24rt Annual DTRA/NNSA Seismic Research Review, Ponte Vedra, FL, 17-19 September. (UNCLASSIFIED)

Garcés, M., D. Drob, and M. Picone, A theoretical study of the effect of geomagnetic fluctuations and solar tides on the propagation of infrasonic waves in the atmosphere. *Geophys. J. International*, 148, 77-87, 2002. (UNCLASSIFIED)

Garcés, M. and C. Hetzer, 2003: Optimizing the Progressive Multi-Channel Correlation Detector for the Discrimination of Infrasonic Sources, 25th Seismic Research Review, Tucson, AZ, 23-25 September. (UNCLASSIFIED)

Garcés, M., C. Hetzer, M. Merrifield, M. Willis, and J. Aucan, 2003: Observations of surf infrasound in Hawai'i, *Geophys. Res. Lett.*, ***30*(24)**, 2264. (UNCLASSIFIED)

Garcés, M., C. Hetzer, M. Willis, and S. Businger, 2003: Integration of infrasonic models with ocean wave spectra and atmospheric specifications to produce global estimates of microbarom signal levels. 25th Seismic Research Review, Tucson, AZ. (UNCLASSIFIED)

Garcés, M., M. Willis, C. Hetzer, and D. Drob, 2004: On using ocean swells for continuous infrasonic measurements of winds in the lower, middle, and upper atmosphere. *Geophys. Res. Lett.* (in press). (UNCLASSIFIED)

Gossard, E. and W. Hooke, 1975: *Waves in the atmosphere*. Elsevier Scientific, New York. 283-385.
Kibblewhite, A., and Cheng Y. Wu, 1996: *Wave interactions as a seismo-acoustic source*. Lecture Notes in Earth Sciences, Springer-Verlag, Berlin. (UNCLASSIFIED)

Kinsman, B., 1965: *Wind Waves.* Prentice Hall, N.J., USA. (UNCLASSIFIED)

Longuet-Higgins, M. S., 1950a: A theory of the origin of microseisms. *Phil. Trans. R. Soc. Lond.*, **243**, 1-35. (UNCLASSIFIED)

Madisetti, V. K. and D. B. Williams, 1998: *The Digital Processing Handbook.* CRC Press, Florida. 14-7pp. (UNCLASSIFIED)

Ponomaryov E. A., A. G. Sorokin, and V. N. Tabulevich, 1998: Microseisms and infrasound: a kind of remote sensing. *Physics of the Earth and Planetary Interiors*, **108**, 339-346. (UNCLASSIFIED)

Posmentier, E., 1967: A theory of microbaroms. Geophys. J. R. Astron. Soc., **13**, 487-501. (UNCLASSIFIED)

Rind, D., 1980: Microseisms at Palisades 3. Microseisms and microbaroms. *J. Geophys. Res.*, **85**, 4854-4862. (UNCLASSIFIED)

Rind, D. Investigation of the lower thermosphere results of ten years of continuous observations with natural infrasound, J. of Atmospheric and Terrestrial Physics, 40, 1199-1209, 1978. (UNCLASSIFIED)

Rogers, W. E. and W. C. O'reilly, 2001: Pacific basin wind-wave models: The generation and propagation of low frequency energy. *Proceedings of Ocean Wave Measurement and Analysis (Waves 2001),* San Francisco, CA, 1-14. (UNCLASSIFIED)

Sanderson, M. Ed., 1993: *Prevailing Trade Winds.* Univ. of Hawaii Press, 12-36.
Saxer, L., 1945: Electrische Messung kleiner atmospharischer Druckshwankingen, *Helv. Phys. Acta.*, **18**, 527. (UNCLASSIFIED)

Saxer, L., 1954: Über Entstehung und Ausbreitung quasiperiodischer Luftdruckschwankungen. *Arch. Meteorol. Geophys. Bioklum.*, **A6**, 451-457. (UNCLASSIFIED)

Shore Protection Manual, Volume 1, Department of Army Waterways Experiment, Corps of Engineers: 1973. (UNCLASSIFIED)

Stevens, J., I. Divnov, D. Adams, J. Murphy, and V. Bourchik, 2002: Constraints on infrasound scaling and attenuation relations from Soviet explosion data. *Pure appl. Geophys.*, **159**, 1045-1062.
Tabulevich, V., 1995: On recordings of global microseismic vibrations and observations of microseisms in shore zones of oceans, *Physics of the Earth and Planetary Interiors*, **91**, 299-305. (UNCLASSIFIED)

Tolman, H. L., 1999: User manual and system documentation of WAVEWATCH-III version 1.19. NOAA/NWS/NCEP/OMB Technical Note Nr. **166**, 110pp. (UNCLASSIFIED)

Tolman, H. L., 2002b: Validation of WAVEWATCH III version 1.15 for a global domain. NOAA/NWS/NCEP/OMB Technical Note Nr. **213**, 33pp. (UNCLASSIFIED)

Vivas Veloso, J., D. Christie, T. Hoffmann, E. Demirovic, P. Campus, M. Bell, A. Molero, A. Langlois, P. Martysevich, J. Carvalho, and A. Kramer, 2002: Status of the IMS Infrasound Network, paper presented at the Infrasound Technology Workshop, De Bilt, Netherlands. (UNCLASSIFIED)

Willis, M., M. Garcés, C. Hetzer, and S. Businger, 2004: Infrasonic observations of open ocean swells in the Pacific: Deciphering the song of the sea. *Geophys. Res. Lett.* (in press). (UNCLASSIFIED)

Willis, M., M. Garcés, C. Hetzer, and S. Businger, 2004: Source Modeling of Microbaroms in the Pacific. Preprints, 84th AMS Annual Meeting. Eighth Symposium on Integrated Observing and Assimilation Systems for Atmosphere, Oceans, and Land Surface (IAOS-AOLS), Seattle, WA, *Amer. Meteor. Soc.*, P2.5. (UNCLASSIFIED)

Willis, M., 2004: Observations and source modeling of microbaroms in the Pacific. M.S Thesis, Dept. of Meteorology, University of Hawaii at Manoa, 63 pp. (UNCLASSIFIED)

Willis, M., M. Garcés, C. Hetzer, and S. Businger, P. Whittman, J. Bhattacharyya (submitted): Source Modeling of Microbarom Signals, J. Geophys. Res. (UNCLASSIFIED)

Wright, C. W., E. J. Walsh, D. Vandemark, W. B. Krabill, A. W. Garcia, S. H. Houston, M. D. Powell, P. G. Black, and F. D. Marks, 2001: Hurricane Directional Wave Spectrum Variation in the Open Ocean. *J. Phys. Oceanogr.*, **31**, 2472-2488. (UNCLASSIFIED)

APPENDIX A

DERIVATION OF BASIC RELATIONSHIPS FOR THE SURFACE WAVE SPECTRUM, ACOUSTIC SOURCE FUNCTION, AND INFRASONIC AMPLITUDE SCALING FOR MICROBAROM SIGNALS

A.1 SURFACE WAVE SPECTRUM

The Wavewatch 3 model outputs the variance density, F, of the surface wave field as a function of frequency, f, and propagation direction, θ. The variance density can be integrated over angle and frequency to provide the total wave energy E,

$$E = \int_0^{2\pi} d\theta \int_0^{\infty} df F(f,\theta). \qquad \text{(A1)}$$

The significant wave height is defined as

$$H_s = 4\sqrt{E}\,. \qquad \text{(A2)}$$

And thus the variance density has units of m^2/(rad*Hz) and it is a measure of the energy in the surface wave field. The phase of each wave component is assumed to be random.
Arendt and Fritz (2000) start with a prescribed amplitude spectrum of the ocean surface wave field given by the cosine Fourier transform

$$g(x,y,t) = \int_{-\infty}^{\infty} dk_x \int_{-\infty}^{\infty} dk_y A(k_x,k_y)\cos(\omega t - k_x x - k_y y + \phi) \qquad \text{(A3)}$$

$$= \int_{-\infty}^{\infty} dk_x \int_{-\infty}^{\infty} dk_y A(k_x,k_y)\cos(\omega t - k_x x - k_y y + \phi)$$

Thus we wish to find a functional relationship between the variance density F (also known as the directional spectrum) and the Fourier coefficient A, which has to have units of m^3.
From Kinsman (1965), Eq. (8.3:1)

$$g(x,y,t) = \int_0^{\infty} \int_{-\pi}^{\pi} \cos(\omega t - k_x x - k_y y + \phi)\sqrt{F(\omega,\theta)}\,d\theta\,d\omega \qquad \text{(A4)}$$

This integral representation reminds us that we are dealing with a Gaussian process, and is the subject of an involved discussion by Kinsman. Since the WW3 model is defined in a grid of frequencies and azimuths, we estimate our wavenumber spectrum as:

$$g(x,y,t) \approx \int_0^{\infty} \int_{-\pi}^{\pi} \cos(\omega t - k_x x - k_y y + \phi)\sqrt{\frac{F(\omega,\theta)}{\Delta\theta\Delta\omega}}\,d\theta\,d\omega$$

The first transformation only concerns the change of variables from frequency to wavenumber,

$$g(x,y,t) \approx \int_0^{\infty} \int_{-\pi}^{\pi} \cos(\omega t - k_x x - k_y y + \phi) \frac{d\omega}{dk} \sqrt{\frac{F(\omega,\theta)}{\Delta\theta\Delta\omega}} d\theta dk \qquad \text{(A5)}$$

$$g(x,y,t) \approx \int_0^{\infty} \int_{-\pi}^{\pi} \cos(\omega t - k_x x - k_y y + \phi) c_g \sqrt{\frac{F(\omega,\theta)}{\Delta\theta\Delta\omega}} d\theta dk$$

where c_g is the group velocity. The second transformation involves a change of coordinates in wavenumber space from polar to rectangular,

$$g(x,y,t) \approx \int_{-\infty}^{\infty} dk_x \int_{-\infty}^{\infty} dk_y \cos(\omega t - k_x x - k_y y + \phi) \frac{c_g}{k} \sqrt{\frac{F(\omega,\theta)}{\Delta\theta\Delta\omega}} \qquad \text{(A6)}$$

For short-period waves, the phase velocity c_s and group velocity c_g are given as

$$c_s = \frac{\omega}{k} = \sqrt{\frac{g}{k}} = \frac{g}{\omega}, \quad c_g = \frac{1}{2} c_s, \qquad \text{(A7)}$$

and the dispersion relation is $\omega^2 = gk$. Comparison of Eq.(A6) with Eq.(A3) yields

$$A(k_x, k_y) = \frac{c_g}{k} \sqrt{\frac{F(k_x, k_y)}{\Delta\theta\Delta\omega}} \qquad \text{(A8)}$$

since the variables in the radical have units of (m s), we see that A has units of m^3, as desired.

A.2 ACOUSTIC SPECTRUM

From Arendt and Fritz (2000) the pressure field radiated by a three dimensional surface wave field into an isotropic half space may be expressed as

$$p_m(x,y,z,t) = \int_{-\infty}^{\infty} dK_x \int_{-\infty}^{\infty} dK_y \int_0^{\infty} dK_z P_k(K_x, K_y, K_z) \exp(\omega_m t - \bar{K} \bullet \bar{R} + \phi), \qquad \text{(A9)}$$

where K is the acoustic wavenumber, ω_m is the angular frequency for the sound field, and R is the spherical radius from the source location to the receiver. The spectrum P_k is given by

$$P_k = \frac{\rho c^6}{64 g^2} K_z K^4 \int_0^{2\pi} A(k_x, k_y) A(k'_x, k'_y) d\theta_\xi \qquad \text{(A10)}$$

where k and k' correspond to the second order, propagating solutions of interacting wave fields with near equal angular frequencies ω and ω' and opposite directions, and

$$K^2 = K_x^2 + K_y^2 + K_z^2 \qquad \text{(A11)}$$

$$K_x = k_x + k'_x,\ \xi_x = k_x - k'_x$$
$$K_y = k_y + k'_y,\ \xi_y = k_y - k'_y$$
$$K_z = \sqrt{\left(\frac{\omega+\omega'}{c}\right)^2 - K_x^2 - K_y^2}\ .$$

The highest spectral amplitude will occur when $K_x = K_y = 0$, or $k' = -k$, and $\omega = \omega'$, and

$$P_k^0 = \frac{\rho c^6}{64 g^2} K^5 \int_0^{2\pi} A(k_x, k_y) A(-k_x, -k_y) d\theta \qquad \text{(A12)}$$

$$\xi_x = 2k_x$$
$$\xi_y = 2k_y$$
$$K = K_z = \frac{2\omega}{c} = \frac{\omega_m}{c}. \qquad \text{(A13)}$$

Where θ is now the directional angle for k specified in equation (1). Using Equations (6) and (8), as well as $\omega_m = 2\omega$,

$$A(k_x, k_y) A(-k_x, -k_y) = \left(\frac{c_g}{k}\right)^2 \sqrt{F(k_x, k_y) F(-k_x, -k_y)} = \left(\frac{4g^2}{\omega_m^3}\right)^2 \sqrt{F(k_x, k_y) F(-k_x, -k_y)}. \qquad \text{(A14)}$$

the peak spectrum amplitude then becomes

$$P_k^0 = \frac{\rho c g^2}{4\omega_m}\left[\int_0^{2\pi} \sqrt{F(k_x, k_y) F(-k_x, -k_y)} d\theta\right] = \frac{\rho c g^2}{4\omega_m} Q_m^0 \qquad \text{(A15)}$$

$$Q_m^0 = \int_0^{2\pi} \sqrt{F(k_x, k_y) F(-k_x, -k_y)} d\theta = 2\int_0^{\pi} \sqrt{F(f, \theta F(f, \theta + \pi))} d\theta \qquad \text{(A16)}$$

the integral can be readily evaluated through either the trapezoidal rule or the parabolic rule. For an even number of intervals n (odd number of discrete points $x_j, j = 0,n$), the parabolic rule states

$$\int_a^b f(x) dx \approx \frac{h}{3}[f(x_0) + 4f(x_1) + 2f(x_2) + \ldots + 4f(x_{n-1}) + f(x_n)],$$

where $h = (b-a)/n$. If n is an odd number (even number of points), we can use the trapezoidal rule.

$$\int_a^b f(x)dx \approx \frac{h}{2}[f(x_0)+2f(x_1)+2f(x_2)+...+2f(x_{n-1})+f(x_n)].$$

After this integration is complete, we have completed the transformation from ocean to sound waves and it is practical to use the acoustic microbarom frequency $\omega_m = 2\omega$.

A.3 PRESSURE SCALING WITH RANGE, INCLUDING THE EFFECTS OF THE STATOSPHERIC WINDS

The atmosphere is a complex environment, and for the purpose of microbarom amplitude determinations it behooves us to start with a simple amplitude scaling relationship that will allow us to estimate relative acoustic levels at a receiver. Stevens et al. (2002) provide an evaluation of various scaling laws that have been derived from nuclear tests, and we use the expression that provided the best fit:

$$P = \frac{P_{ref}}{R^{1.36}} 10^{0.019v}$$

where the reference pressure P_{ref} is relative to the source location, the range R is in km, and the stratospheric wind speed v at 50 km along the propagation direction is given in m/s. A source magnitude may be defined as

$M_l = log_{10}(P_{ref})$,

and used to plot the microbarom source spectrum amplitude as a function of global location. However, this expression does not account for the substantial travel time it may take for the signal to reach the station, and the fact that the ocean wave field would have changed during that travel time. Although the Stevens formula was used for preliminary evaluations of the predicted infrasound field, the results were not satisfactory and are not presented in this document.

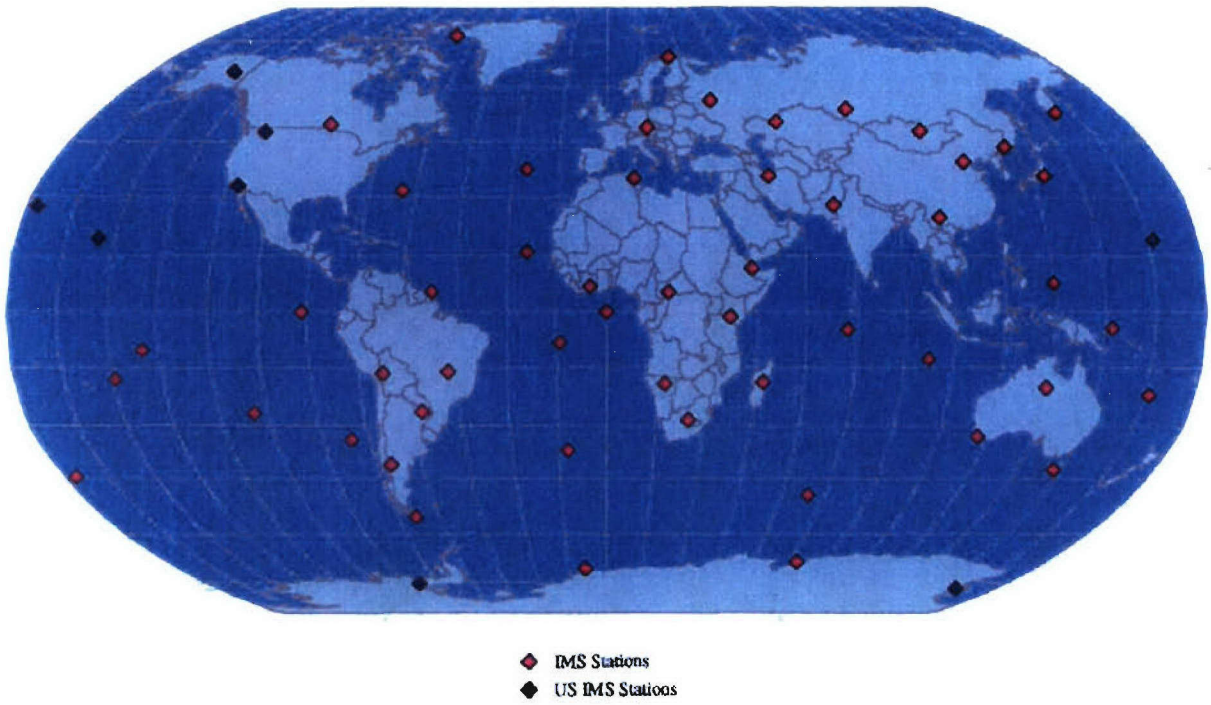

Figure A-1. Infrasound network of the International Monitoring System.

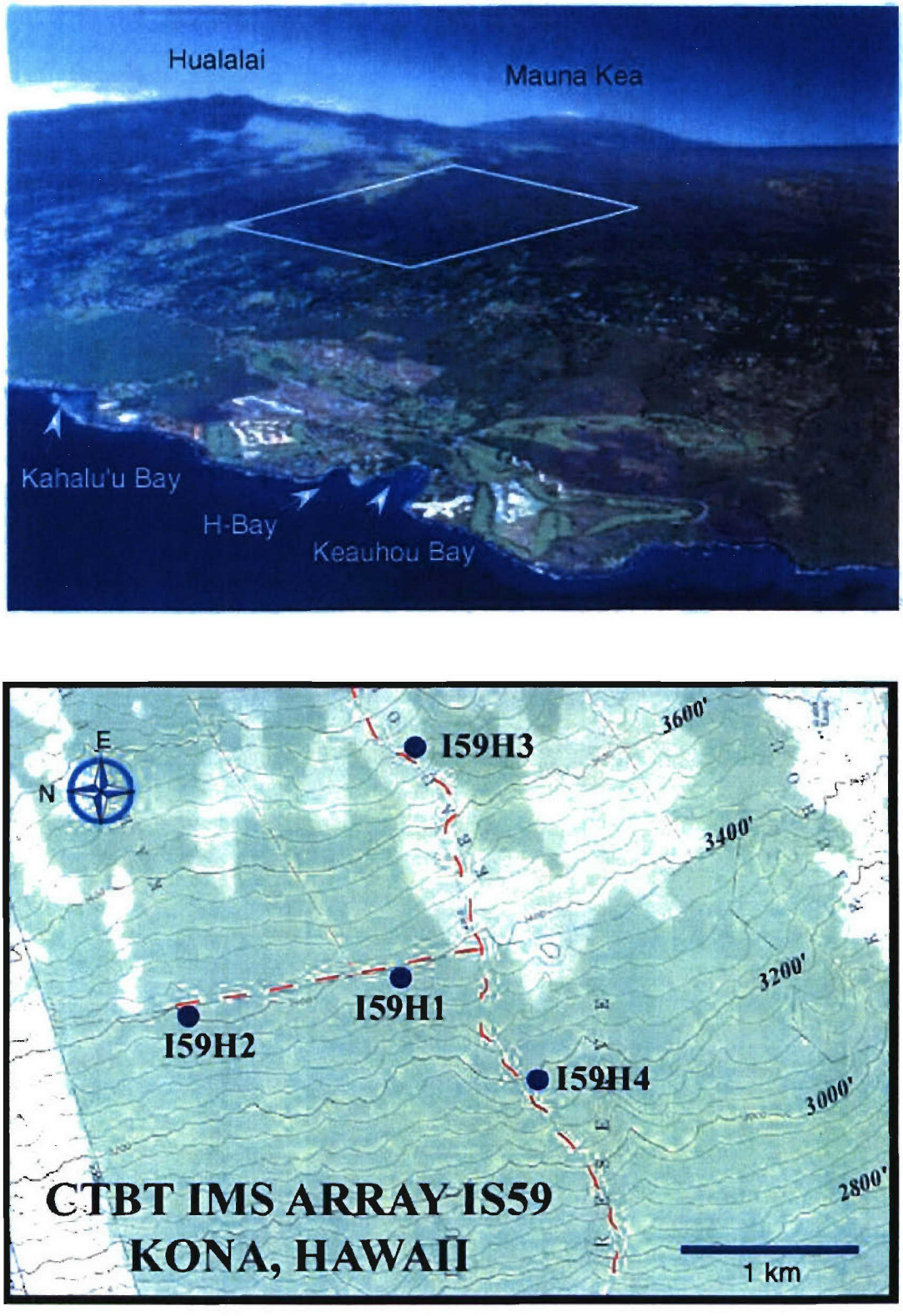

Figure A-2. Geographic location of infrasound array near Kona, Hawaii (19.5915, 155.8936 W). Blue dots on bottom figure represent microphone location.

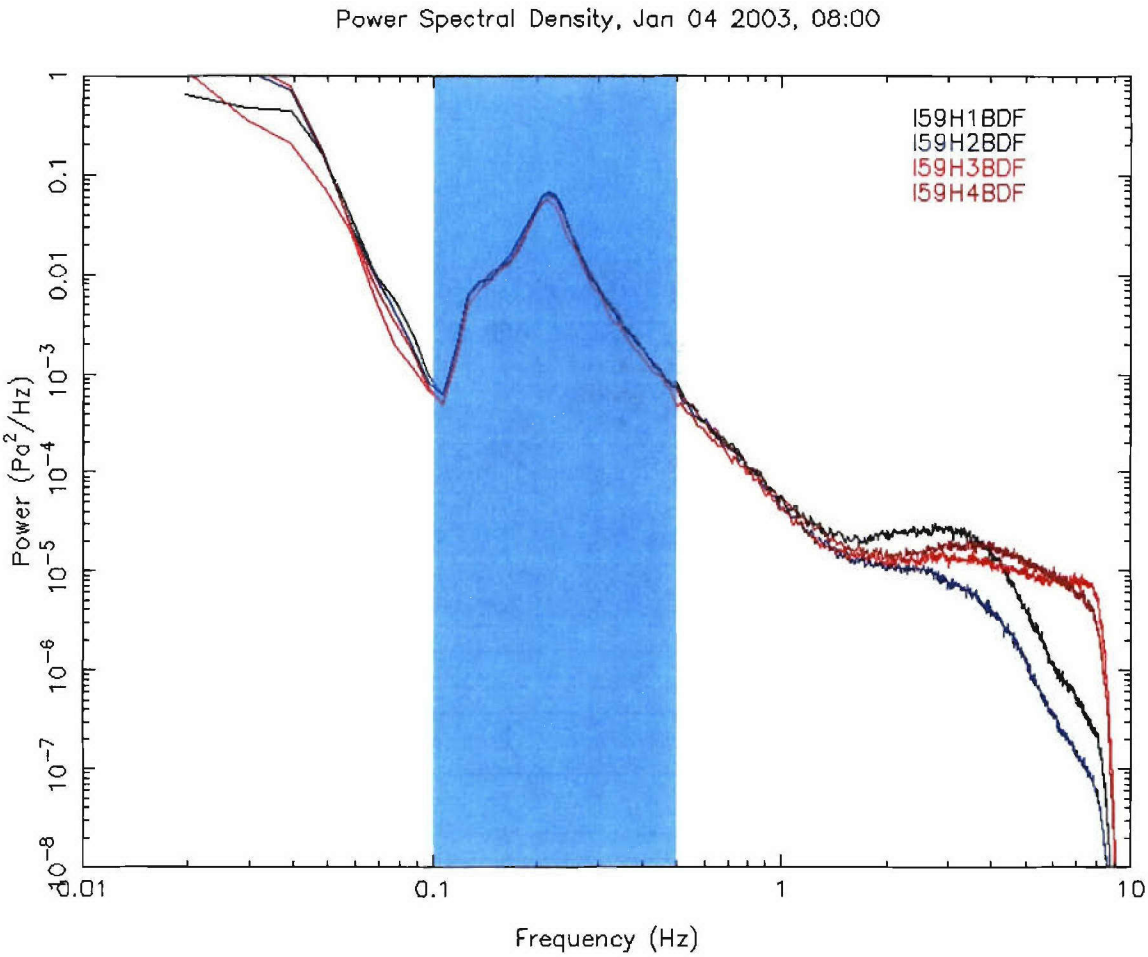

Figure A-3. Acoustic power spectral density observed at I59US site on January 4, 2003 18Z (8am Local). Colored lines represent power observed by the four components of the infrasonic array. Power (Pa^2/Hz) is on the vertical axis, acoustic frequency (Hz) is on the horizontal axis. Blue shaded region represents microbarom frequency range. The ~0.2 Hz peak is common throughout the year at I59US, which theoretically corresponds to ocean waves of 10 sec.

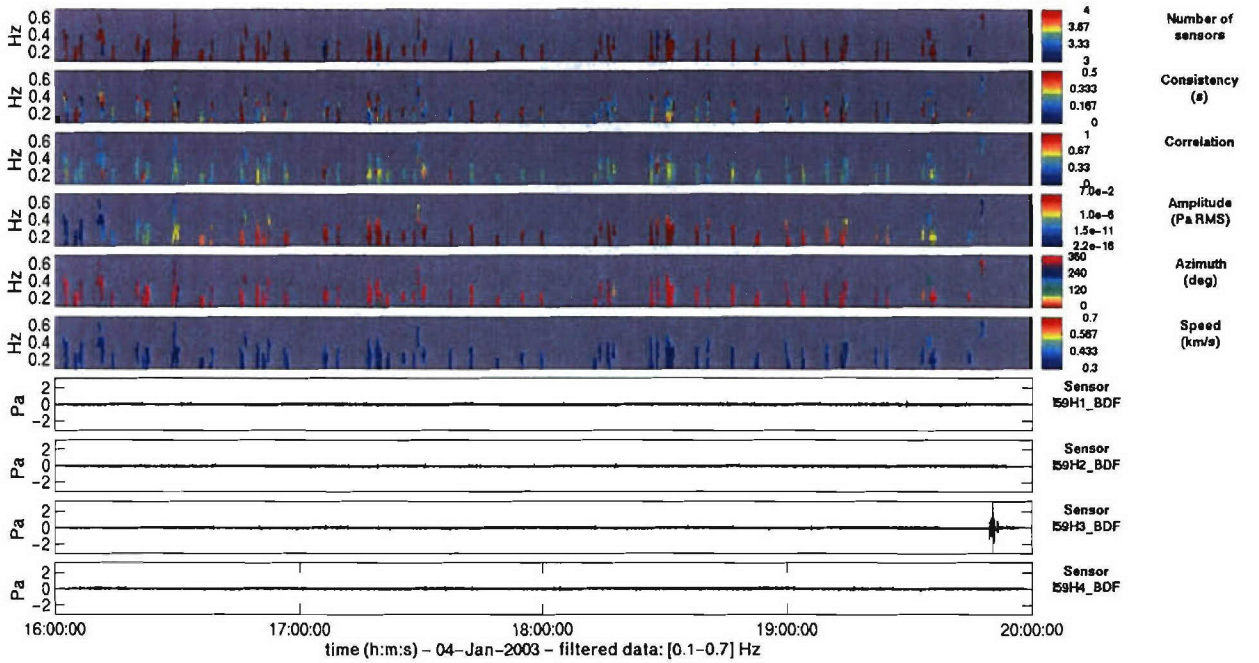

Figure A-4. Graphical PMCC window from Jan. 4, 2003 microbarom event.

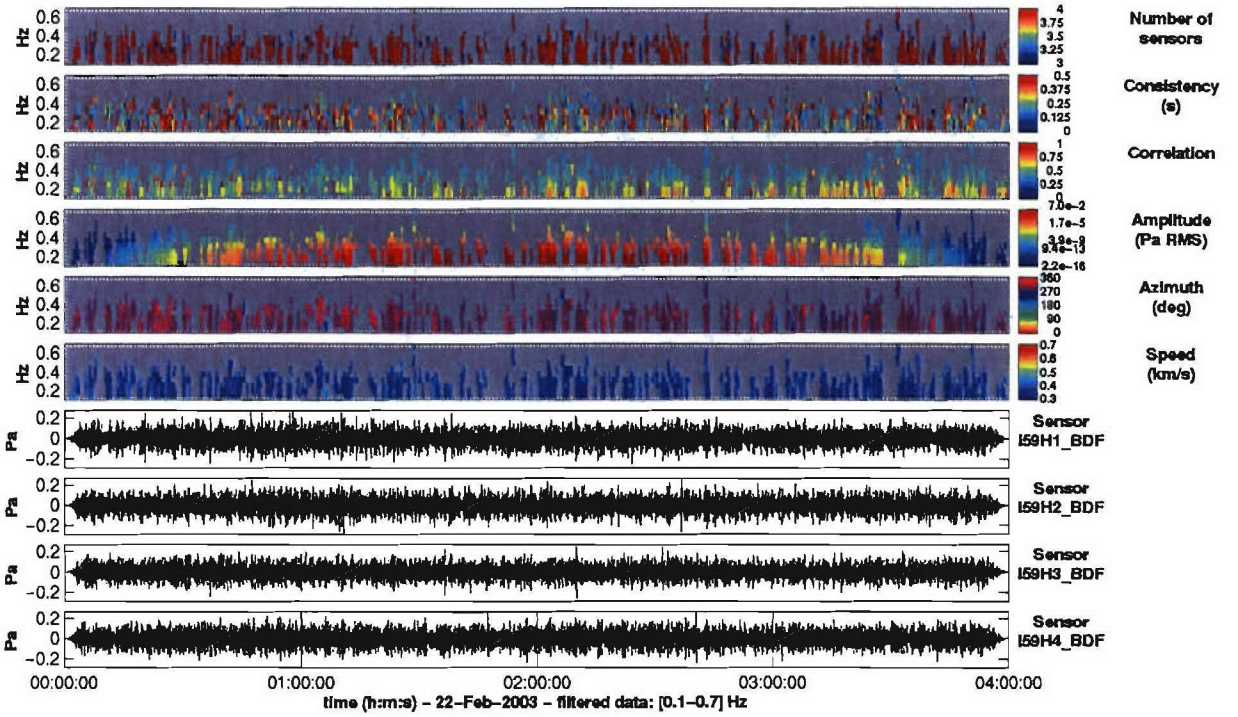

Figure A-5. Graphical PMCC window from Feb. 22, 2003 microbarom event.

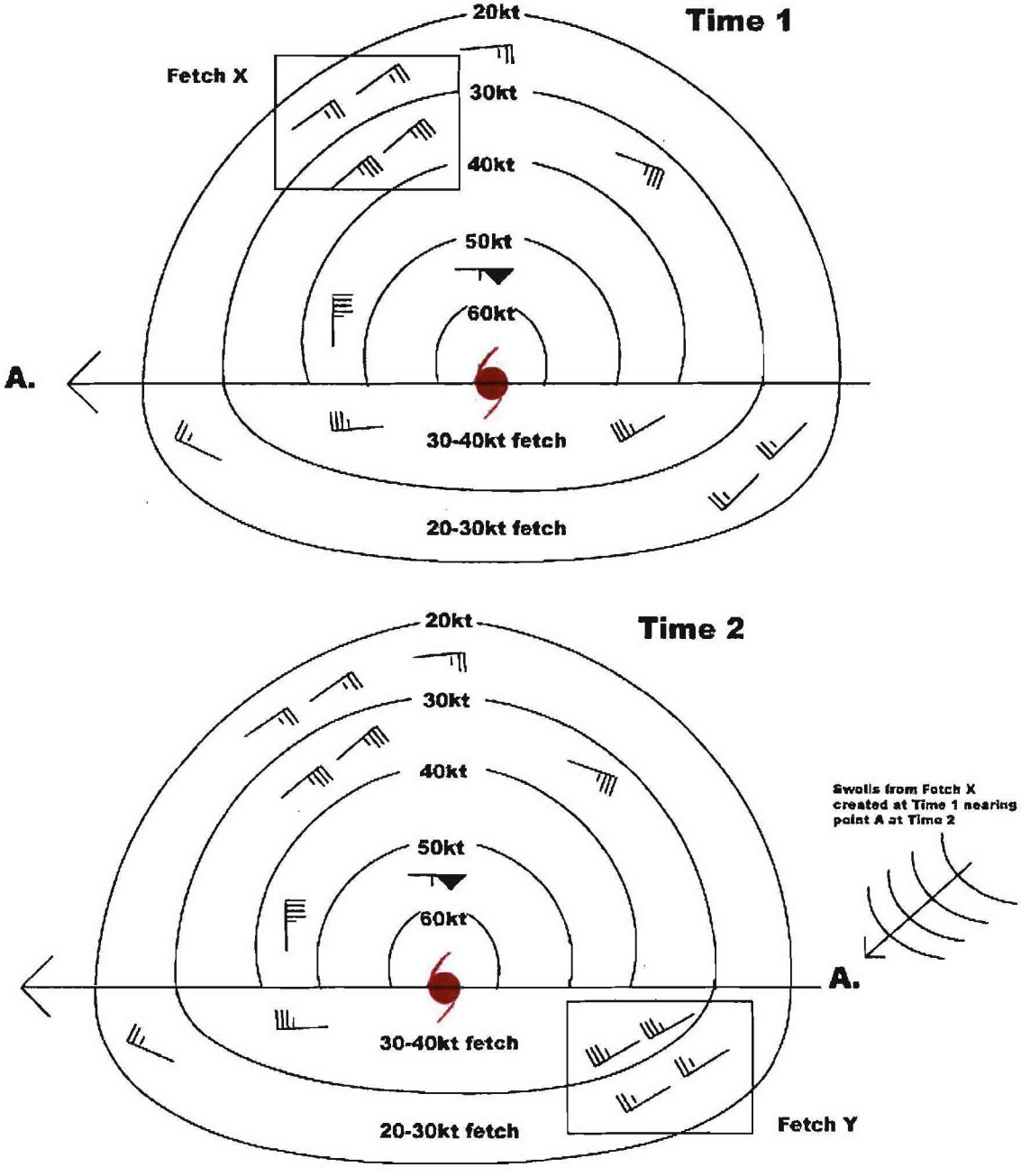

Figure A-6. Simplified, idealized flow around tropical cyclone (or mid-latitude low) "Z" moving west at 20kt in northern hemisphere. In the top figure (Time 1), notice that Fetch X is pointed in the direction of point A. In the bottom figure Fetch Y is pointed in the direction of point A as well, but a different Time 2. Note that Fetch X and Y are nearly identical in magnitude and fetch length and also pointed in nearly opposite directions. Therefore, the ocean waves these two fetches create will contain nearly identical amplitudes and frequencies and will propagate in nearly equal but opposite directions. Amplitude will decay but frequency and direction will remain constant.

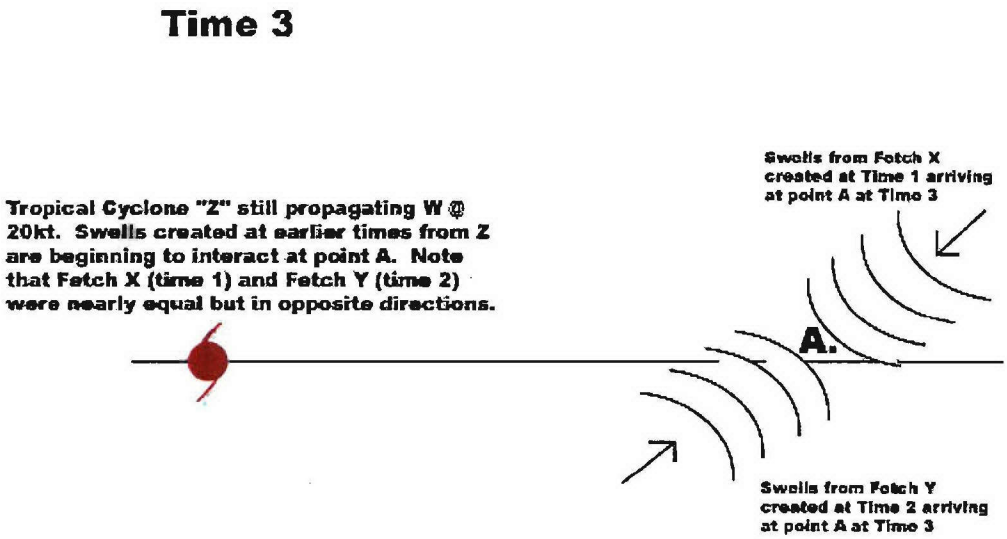

Figure A-7. Swell trains of nearly identical frequencies and in nearly equal but opposite direction meet at point A during Time 3. This scenario supports efficient generation of Infrasound in the 0.1-0.5 Hz band. Regardless of the amplitudes of the interfering wave trains, acoustic radiation will still occur (Arendt and Fritts, 2000).

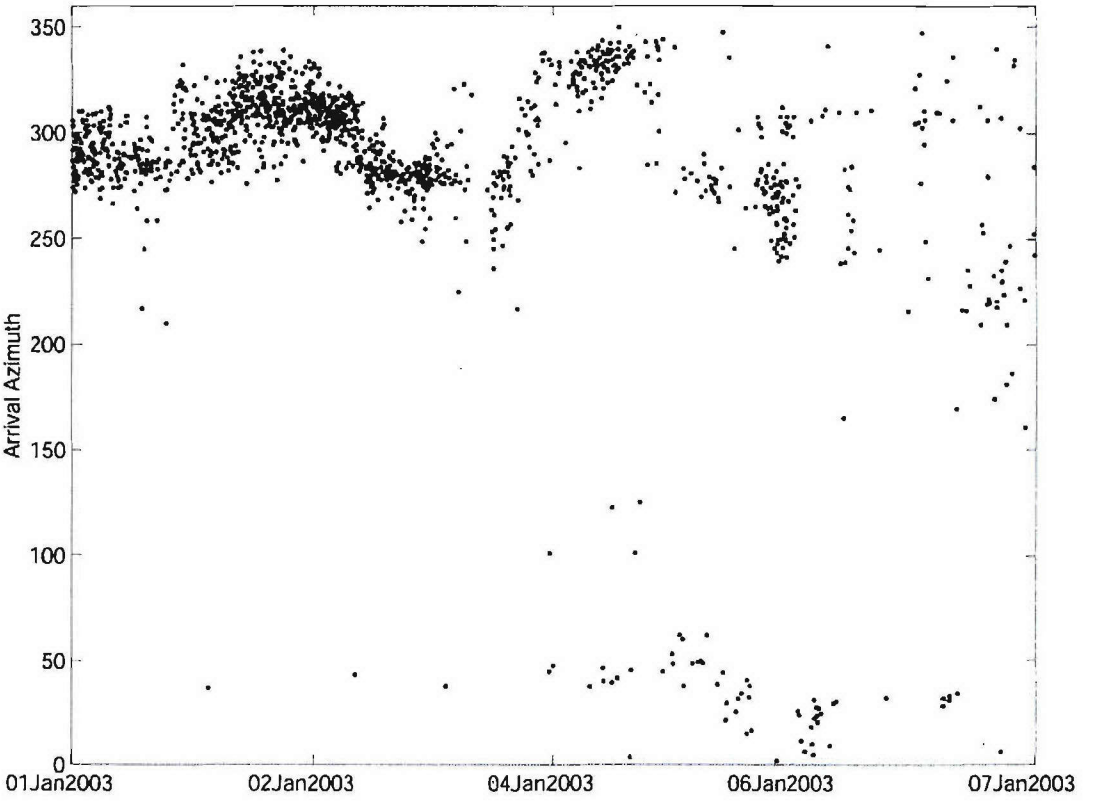

Figure A-8. Arrival azimuth of coherent microbaroms at I59US from January 1-7, 2003. Arrival azimuth is on the vertical axis going clockwise from north (0° to 360°).

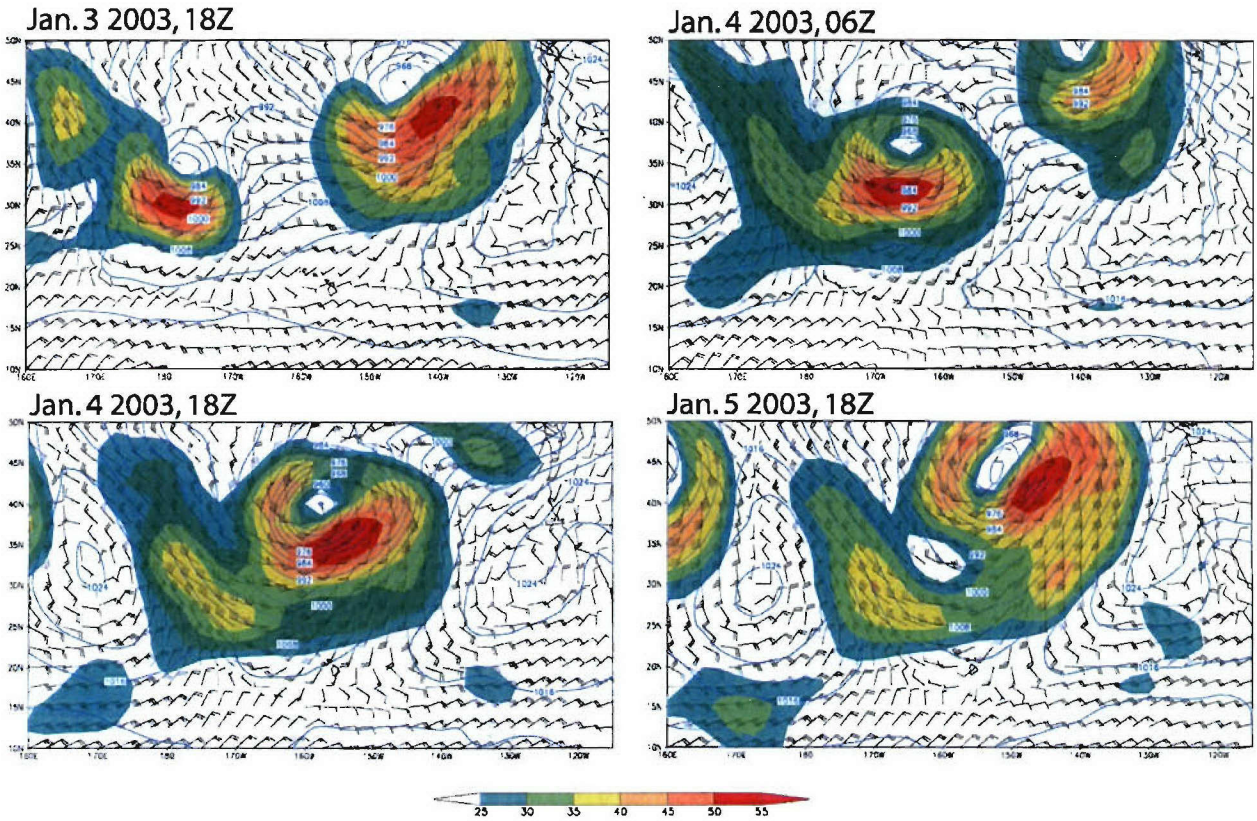

Figure A-9. Analyses of surface pressure (mb) and surface winds (kt) from January 3, 2003 18Z through January 5, 2003 06Z.

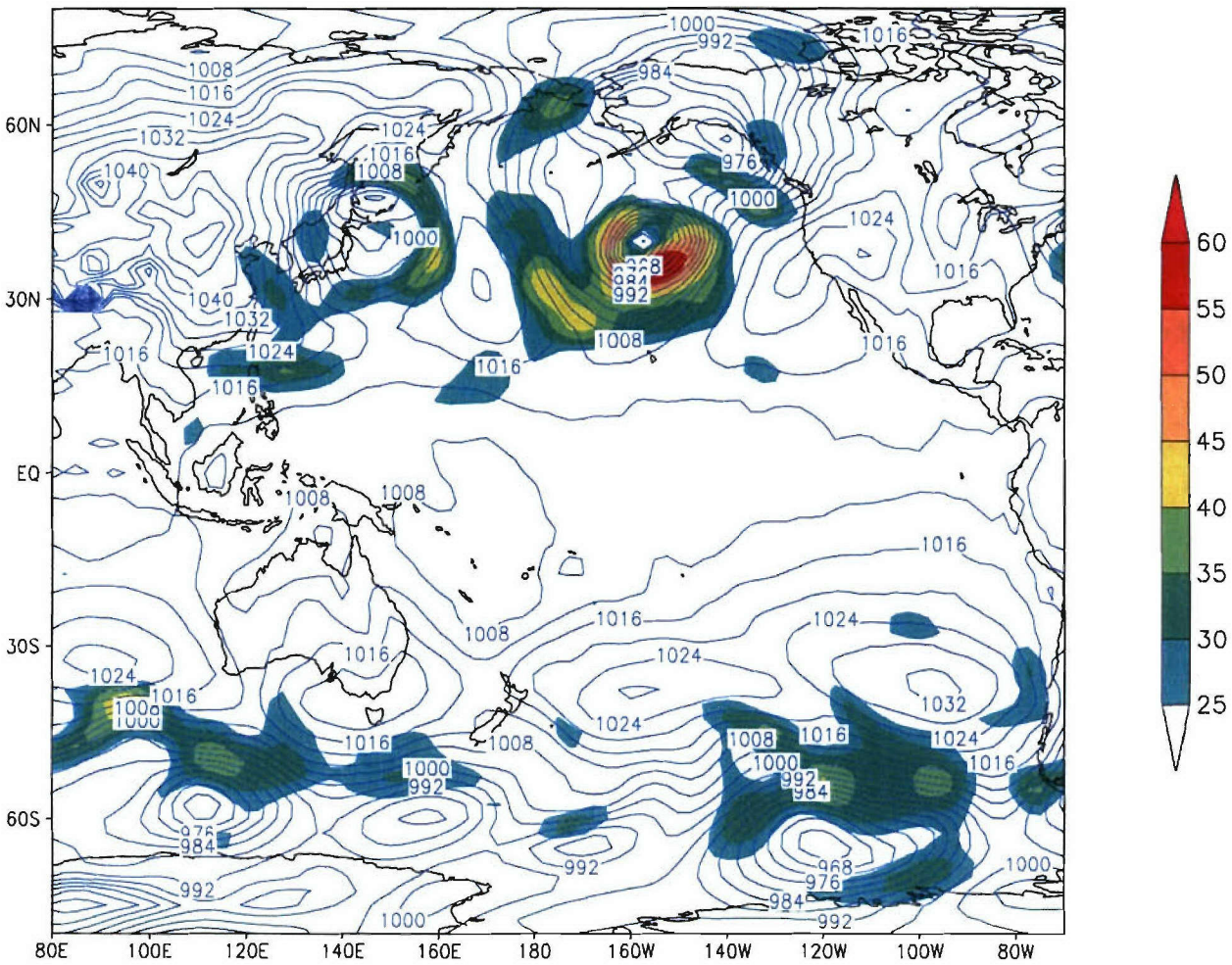

Figure A-10. Analysis of surface pressure (mb) and isotachs (kt, shaded) on January 4, 2003 18Z.

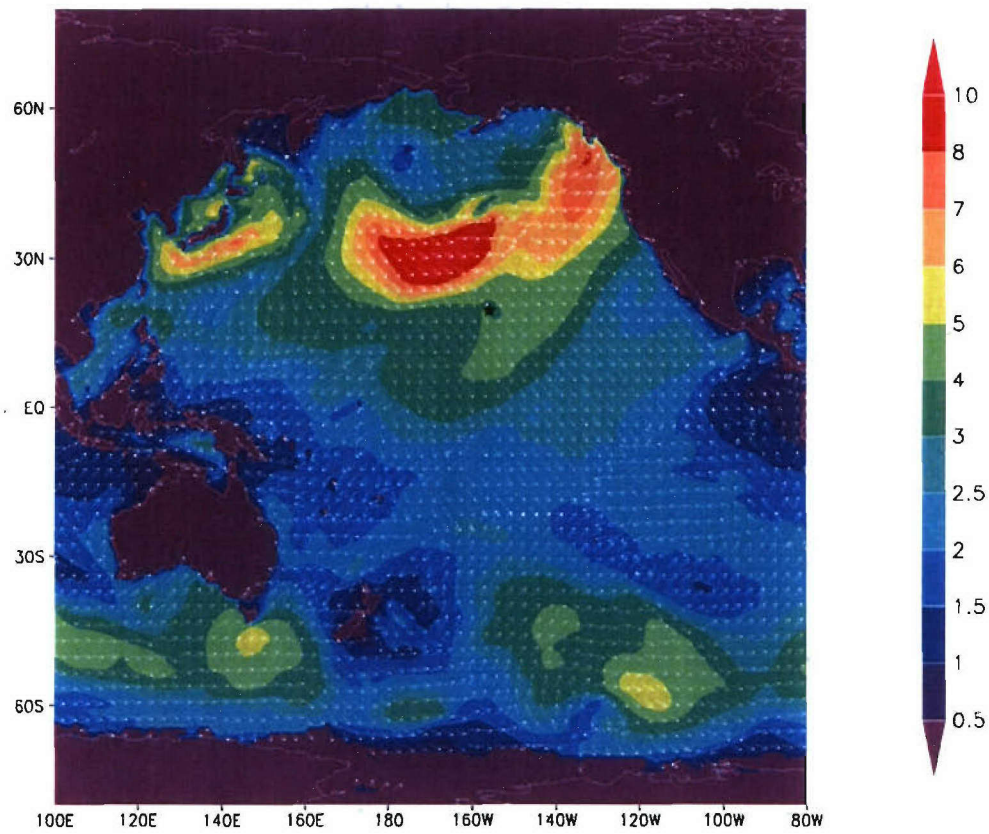

Figure A-11. WW3 Significant wave heights (m, shaded) and mean propagation direction vectors (towards) for January 4, 2003 18Z. Black star represents location of I59US array.

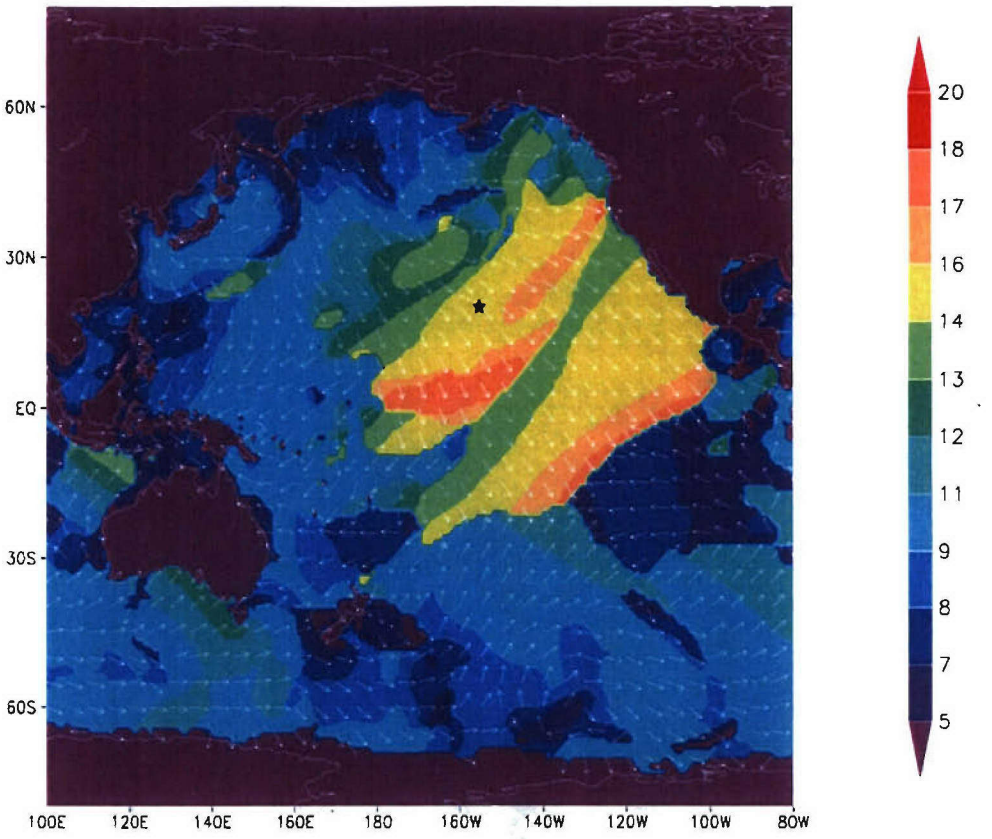

Figure A-12. WW3 Peak periods in seconds (shaded) and directions for January 4, 2003 18Z.

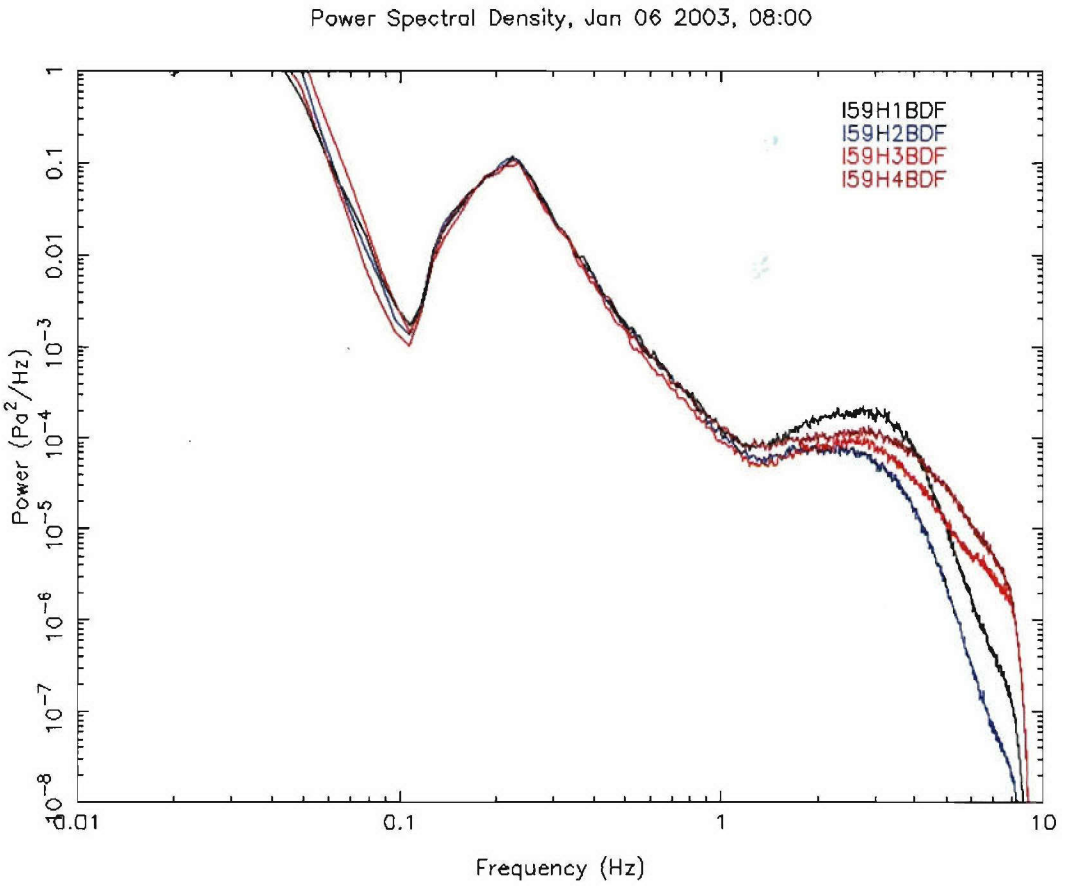

Figure A-13. Acoustic power spectral density observed at I59US site on January 6, 2003 18Z (8am Local). Colored lines represent power observed by the four components of the infrasonic array.

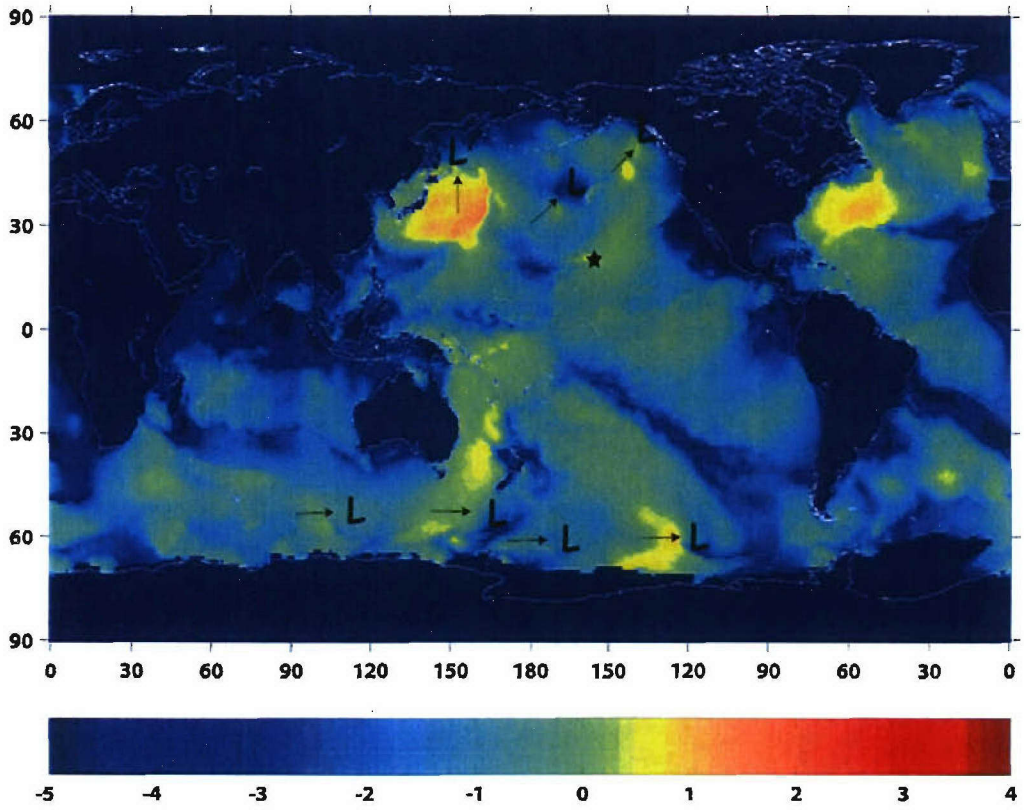

Figure A-14. Base 10 logarithm of the magnitude of the acoustic source pressure spectrum (Pa * m^3) with frequency 0.197 Hz, corresponding to ocean waves interacting with periods of ~ 10 s (produced by equation 4 from spectral output given by WW3) on 01/04/03 18Z. Location of surface low-pressure centers indicated with "L" and storm propagation directions are indicated with arrows.

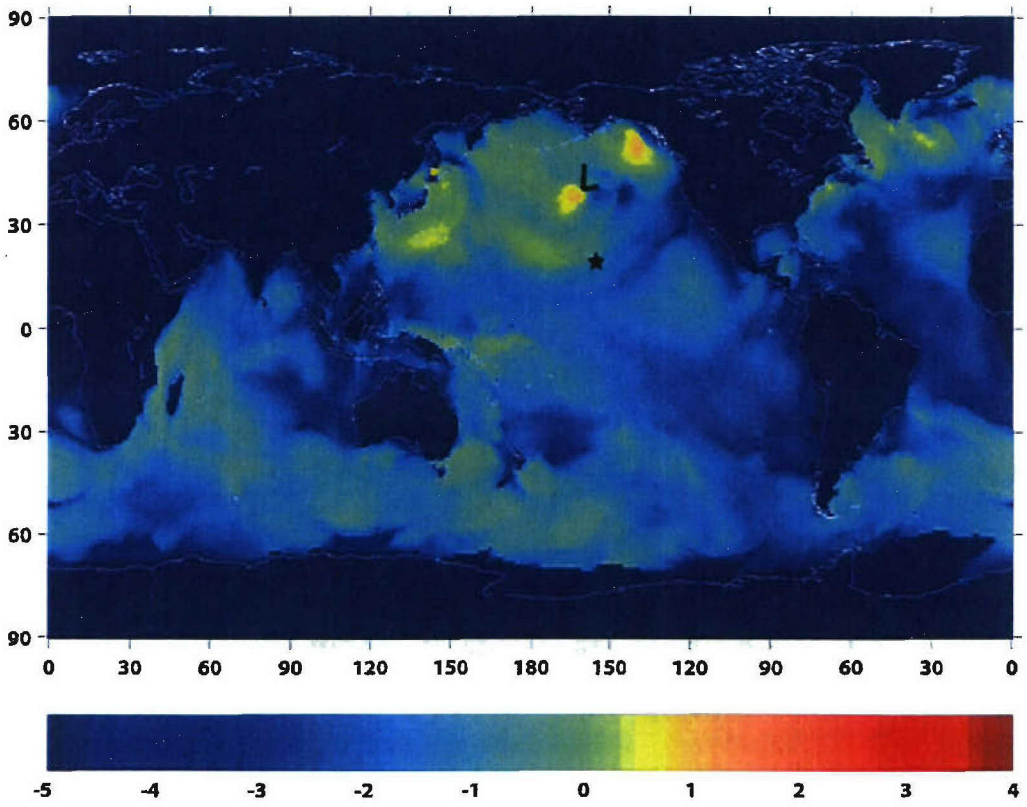

Figure A-15. Base 10 logarithm of the magnitude of acoustic source pressure spectrum (Pa * m^3) with frequency 0.122 Hz, corresponding to ocean waves interacting with periods of ~ 16.4 s on 01/04/03 18Z. Center of strong storm north of Hawaii indicated by "L".

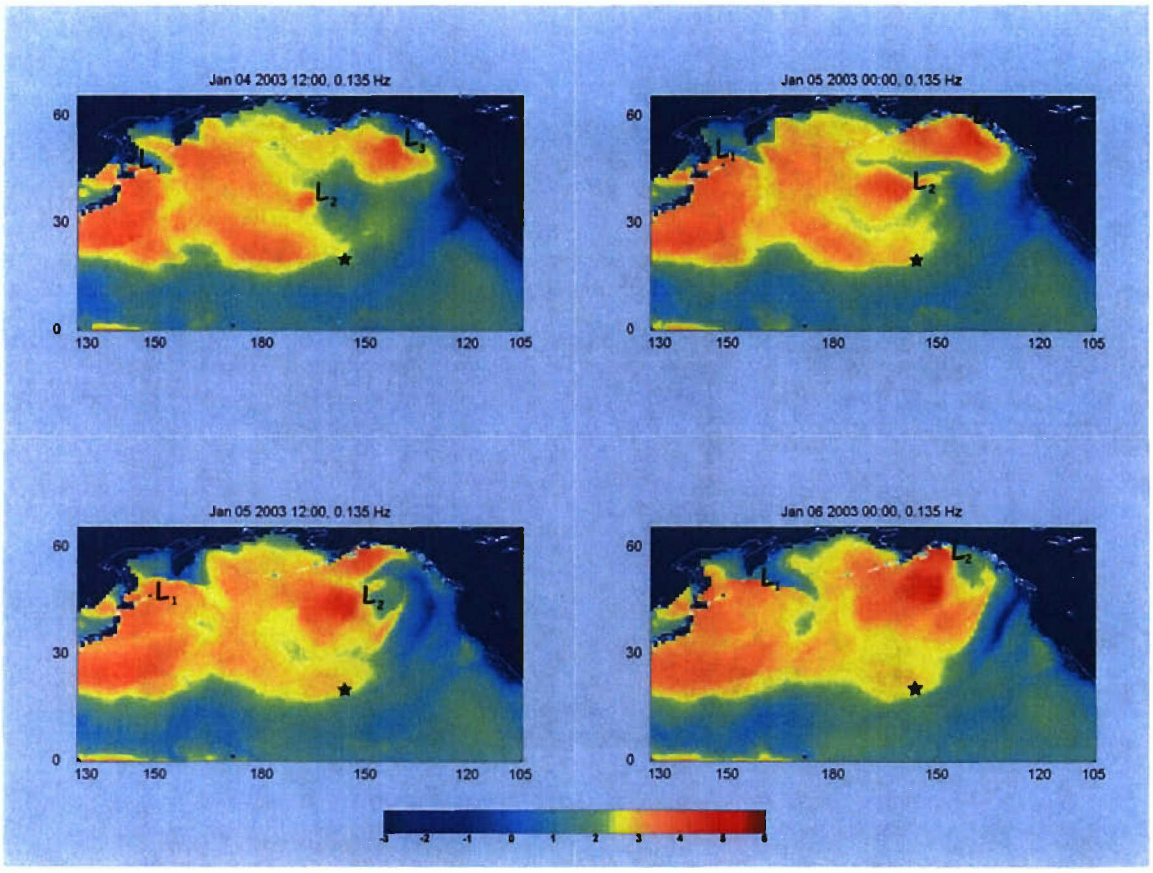

Figure A-16. Acoustic source pressure (Pa * m³, log base 10) with frequency 0.135 Hz from Jan. 4-6, 2003. Corresponds to ocean waves interacting with periods of ~ 14.8 s. The three lows in the North Pacific during this time are tagged L_1, L_2, L_3.

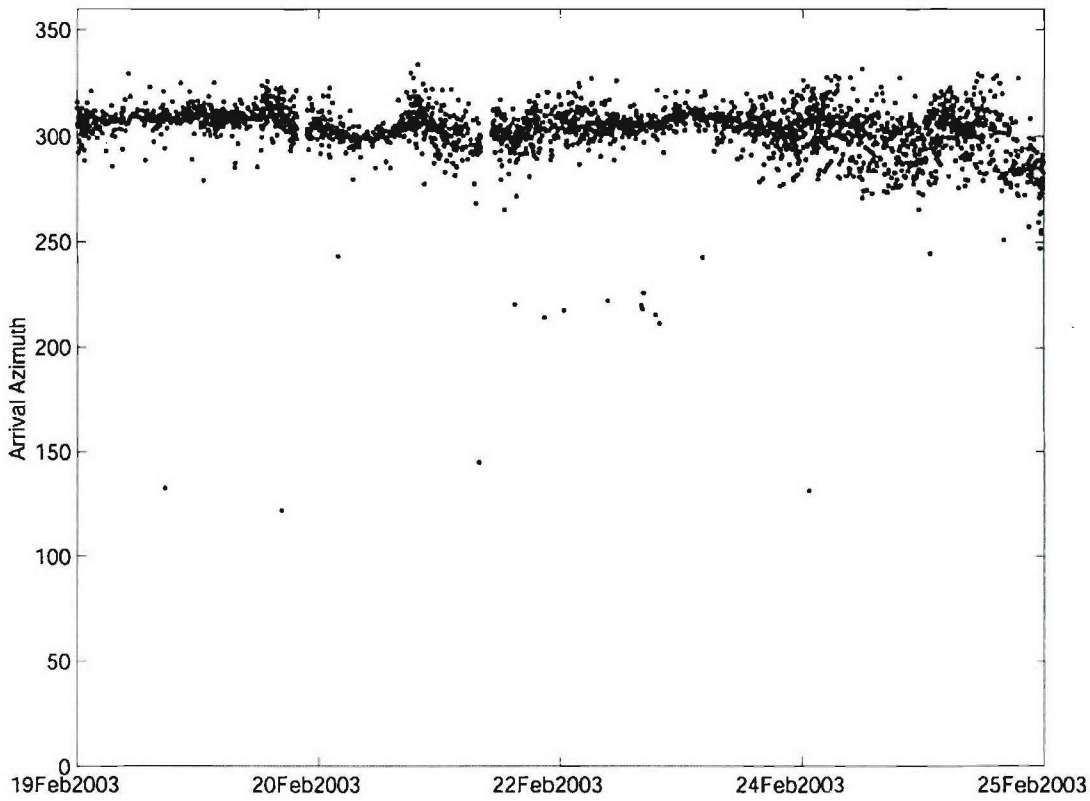

Figure A-17. Arrival azimuth of coherent microbaroms at IS59 from February 19-25, 2003. Arrival azimuth is on the vertical axis going clockwise from north (0° to 360°).

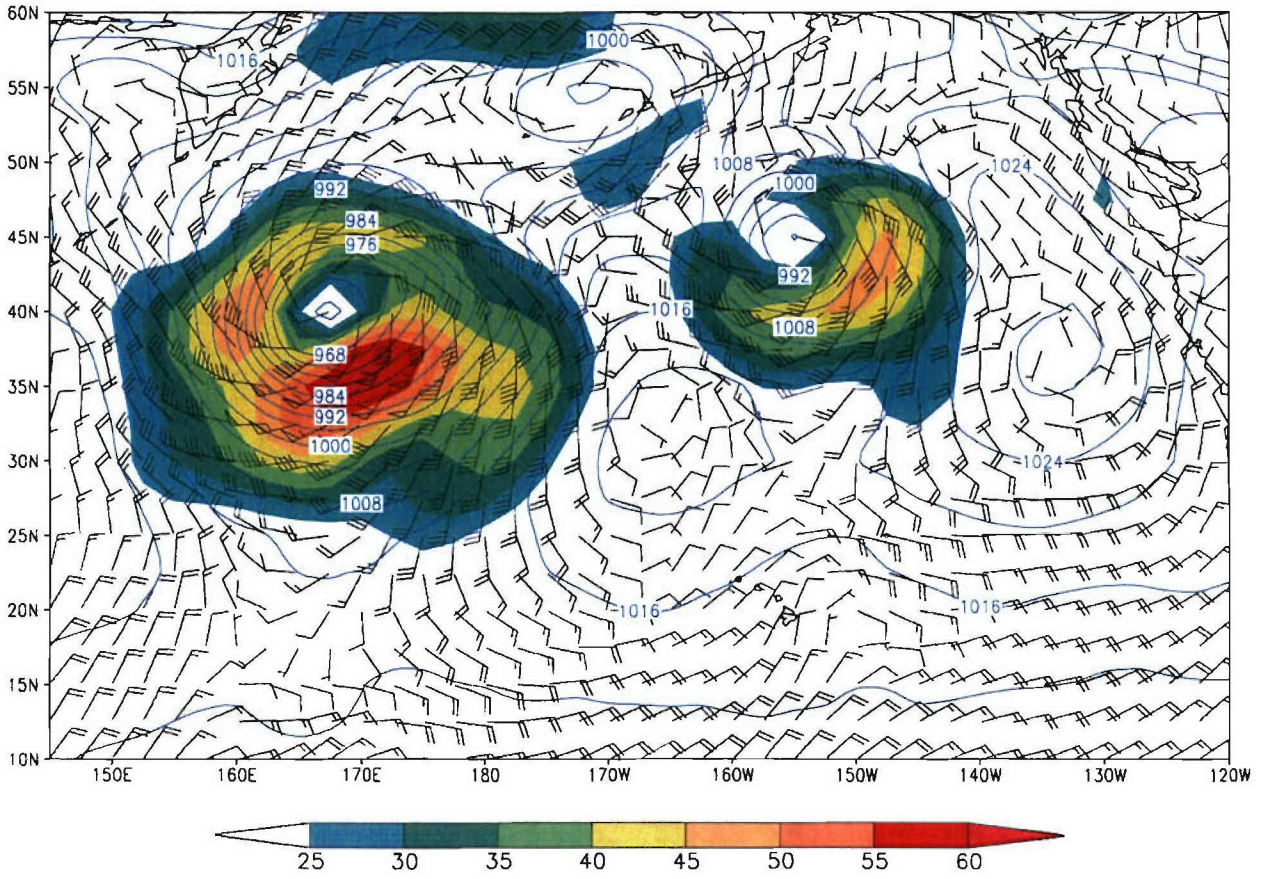

Figure A-18. Analysis of surface pressure (mb) and isotachs (kt, shaded) on February 22, 2003 00Z.

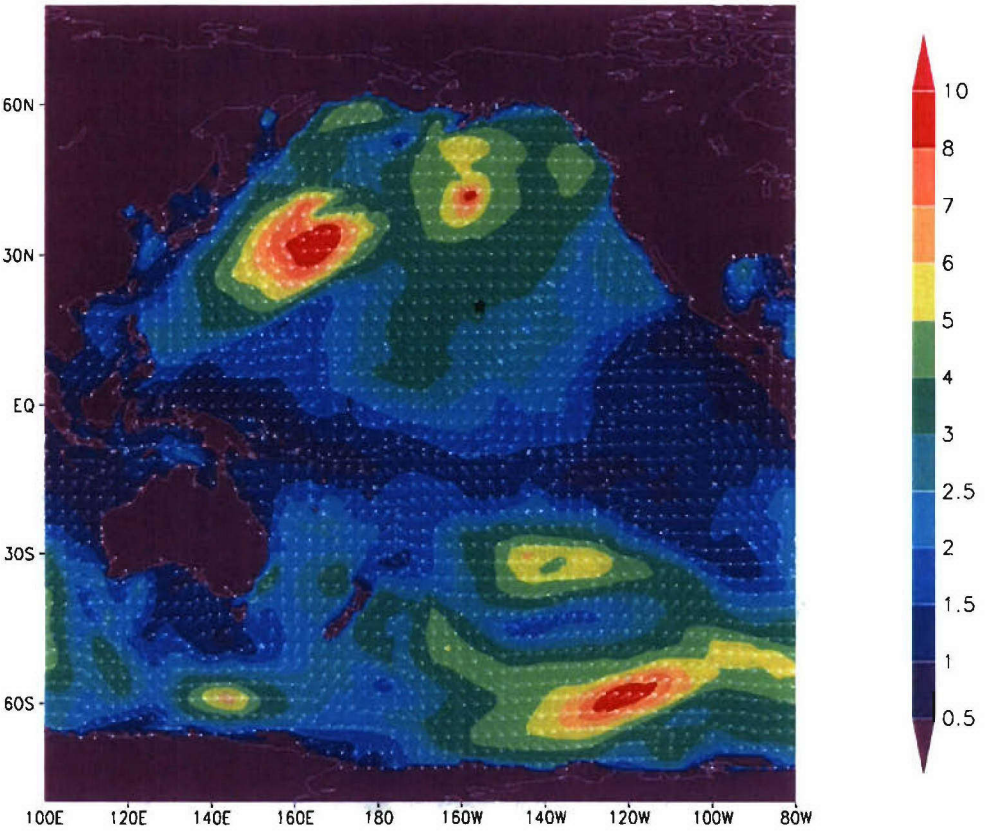

Figure A-19. WW3 Significant wave heights (m, shaded) and mean propagation direction vectors (towards) for February, 22 2003 00Z. Black star represents location of I59US array.

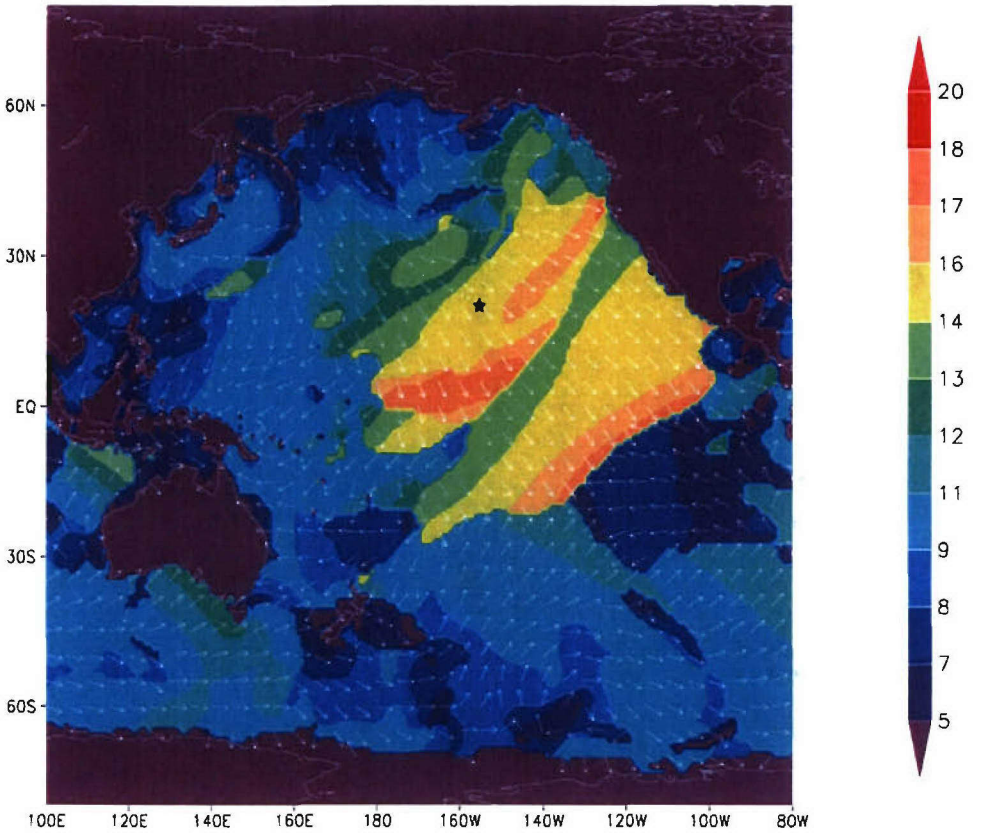

Figure A-20. WW3 Peak periods (shaded) in seconds and directions for February 22, 2003 00Z.

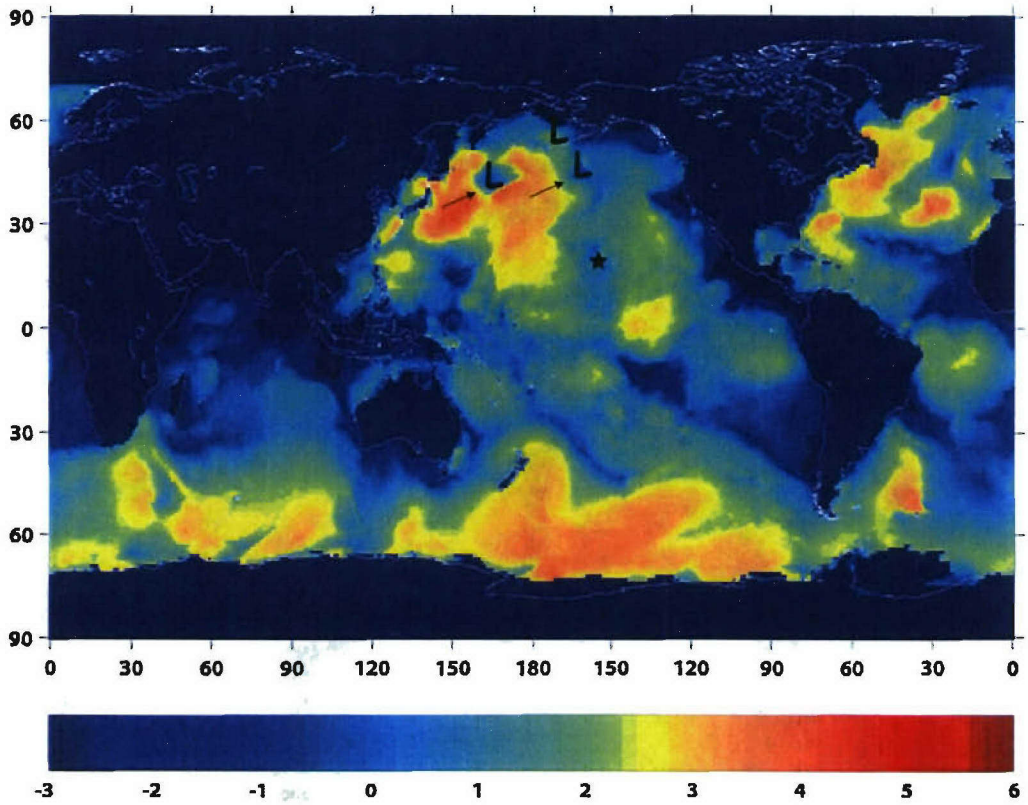

Figure A-21. Base 10 logarithm of the magnitude of the acoustic source pressure (Pa * m^3) with frequency 0.197 Hz, corresponding to ocean waves interacting with periods of ~ 10 s (produced by equation 4 from spectral output given by WW3) on 02/22/03 00Z. North Pacific low pressure centers and propagation direction indicated with L's and arrows, respectively. The low just north of the Aleutian Islands was moving very little.

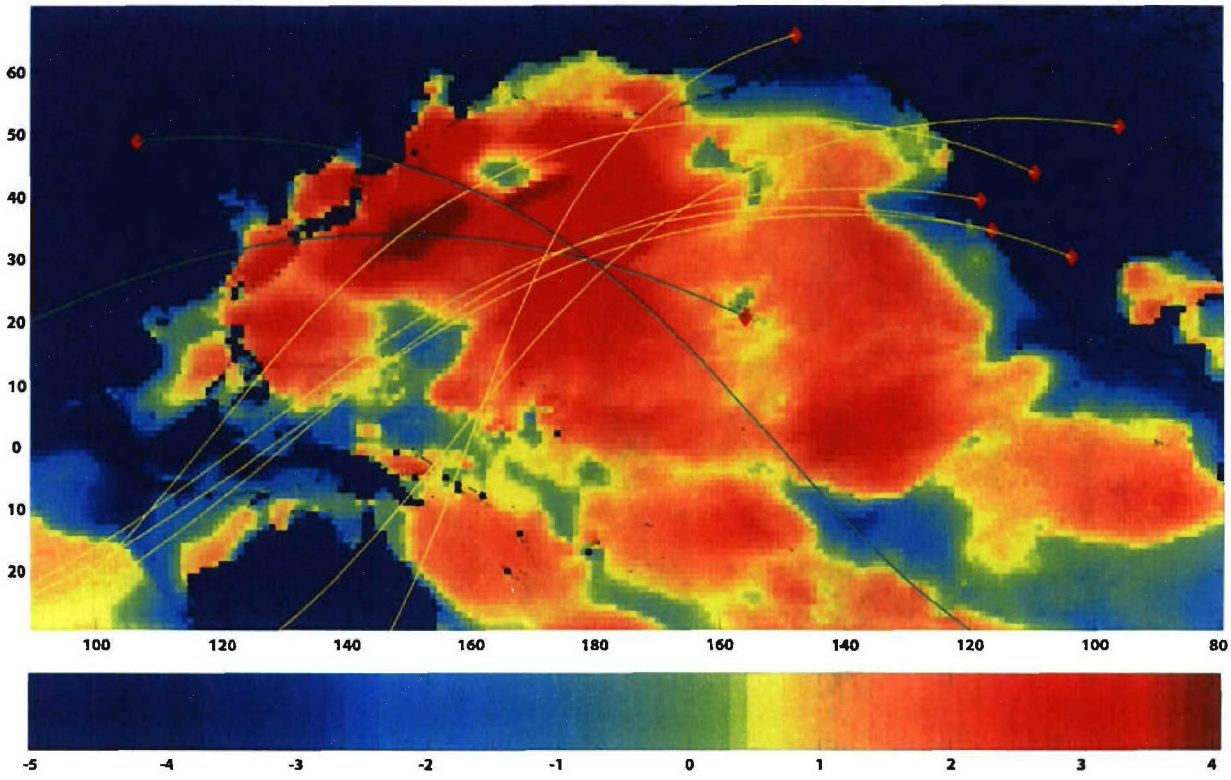

Figure A-22. As in Fig. 20 but reshaded to clarify peak regions. Red shading represents high pressure values while blue shading represents low pressure values. Great circle paths overlaid correspond to the measured microbarom azimuths of Feb. 22, 2003 00Z REB event.

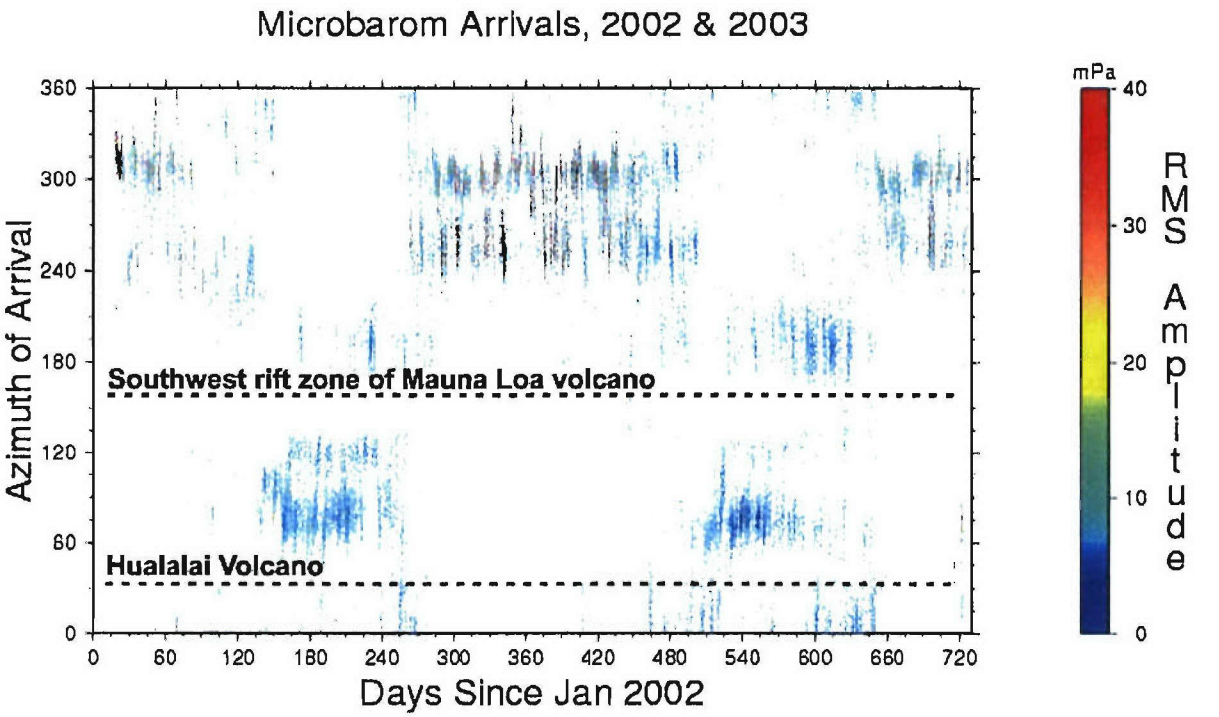

Figure A-23. Time series of coherent microbarom arrivals at the I59US site for 2002 and 2003. Volcano shadow zones overlaid with dotted lines. Note the decrease in amplitude observed during Summer.

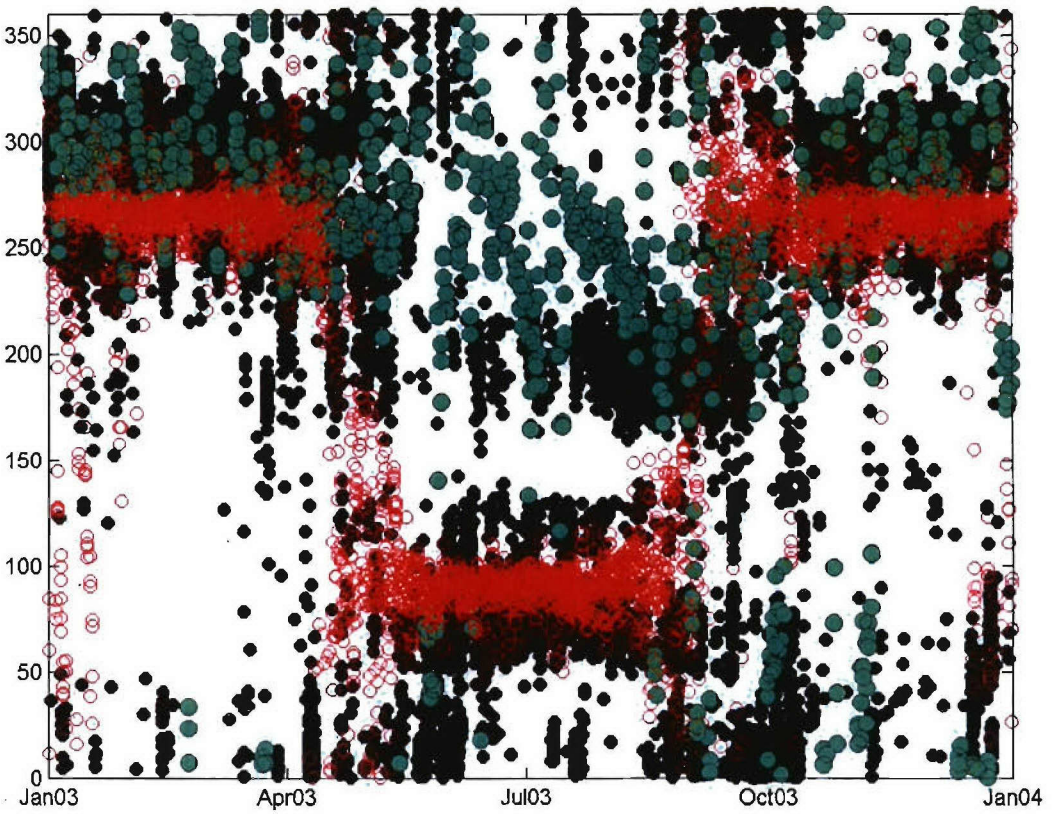

Figure A-24. Coherent microbarom arrival (black circles) and wind arrival azimuths, clockwise from North, at the Hawaii array. The transparent circles with the red rim represent the winds between 50-70 km and the green circles represent the winds between 10-20 km evaluated at 18UT. The dominant wind directions match the seasonal variability for some of the arrivals, except for the arrivals from the Southern hemisphere during the Austral winter. These S swells are large, consistent, and powerful, and may overwhelm the 10s period swell energy.

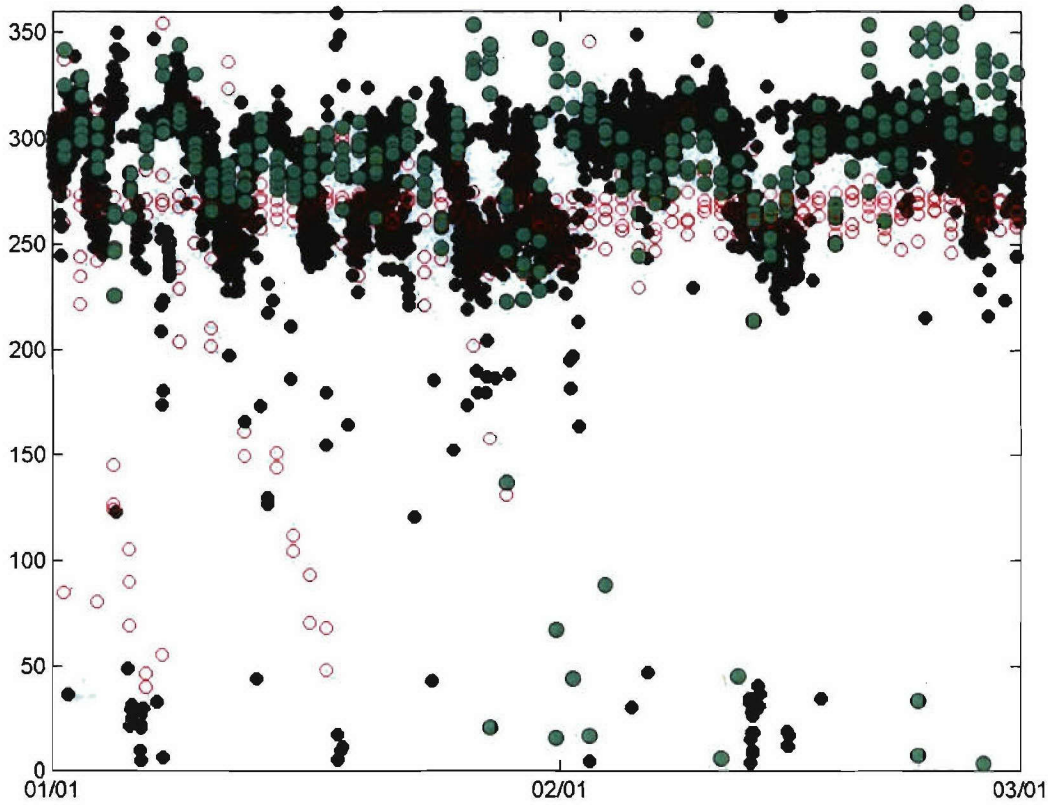

Figure A-25. Same as Figure A-5 but only for January and February, and showing a match between the tropospheric wind direction and a number of the microbarom arrival azimuths.

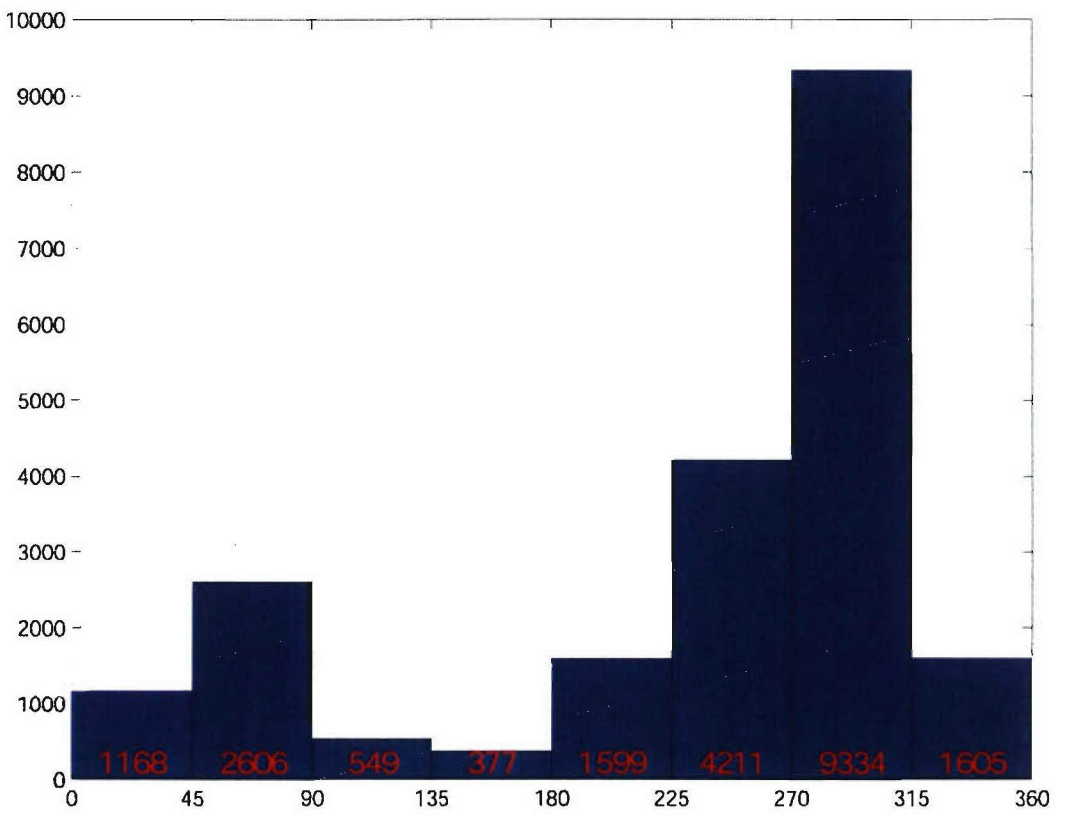

Figure A-26. Total microbarom arrivals at I59US during 2003. Arrival azimuth in degrees is located on the x-axis, total arrivals on the y-axis.

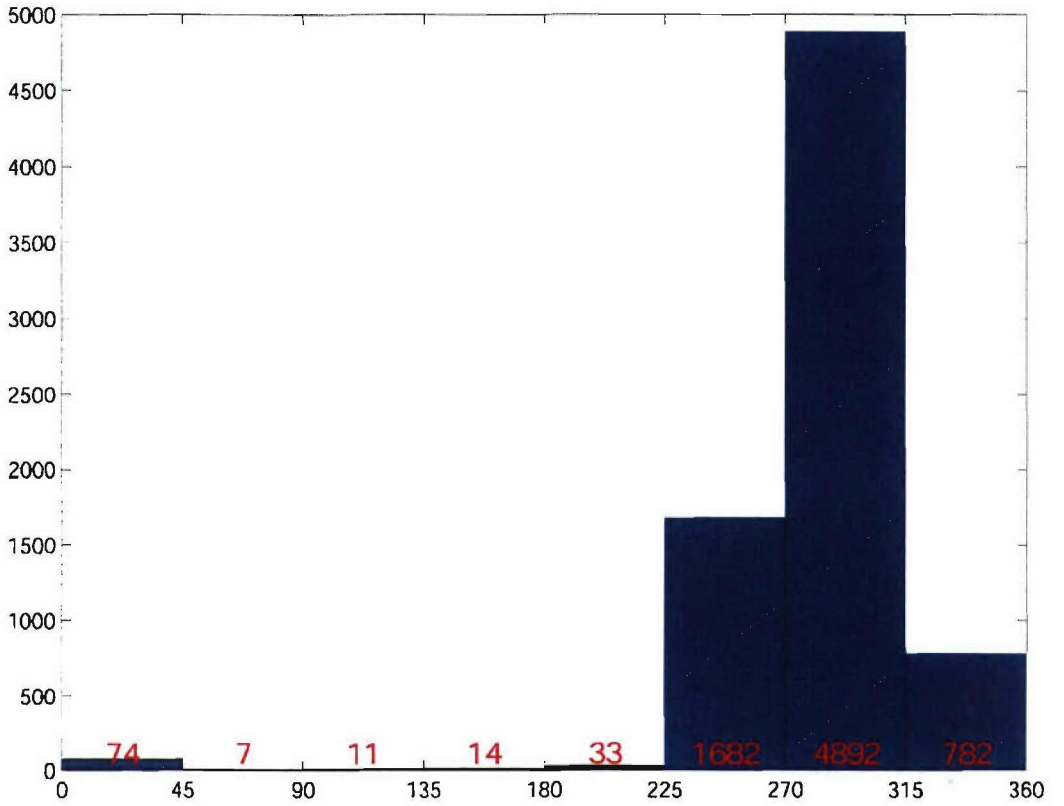

Figure A-27. Total microbarom arrivals at I59US during peak boreal winter months (December 2002, January & February 2003). Arrival azimuth in degrees is located on the x-axis, total arrivals on the y-axis.

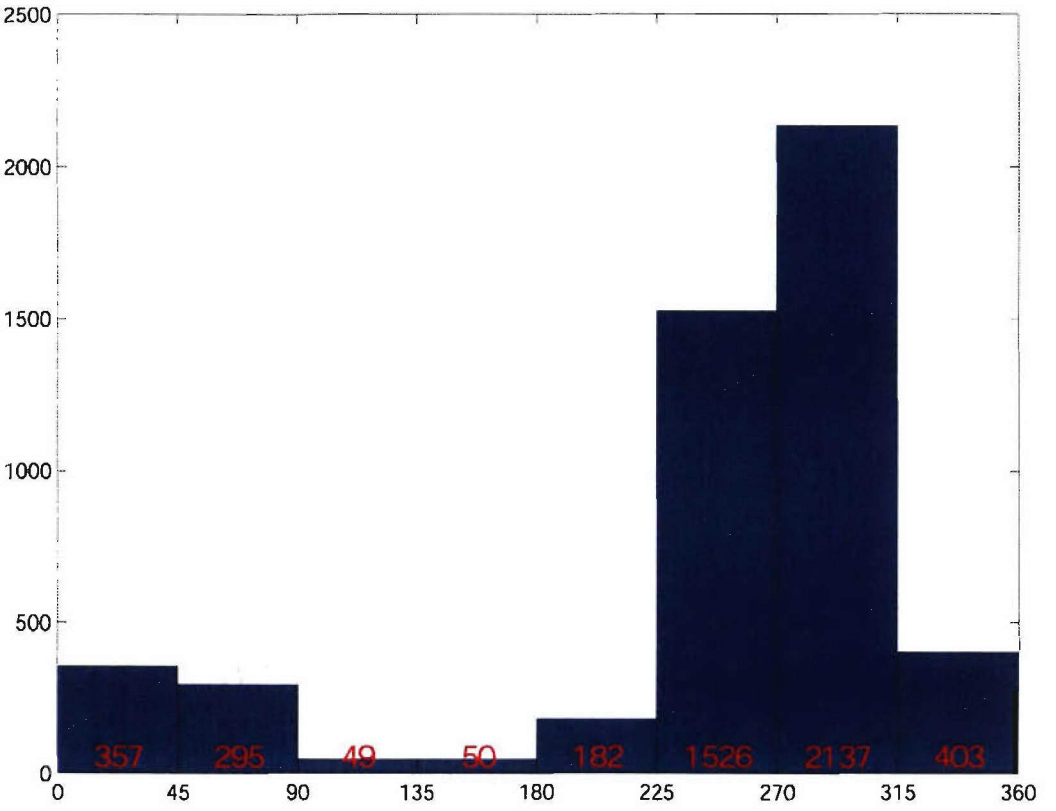

Figure A-28. As in Figure A-5 for months March, April, May 2003.

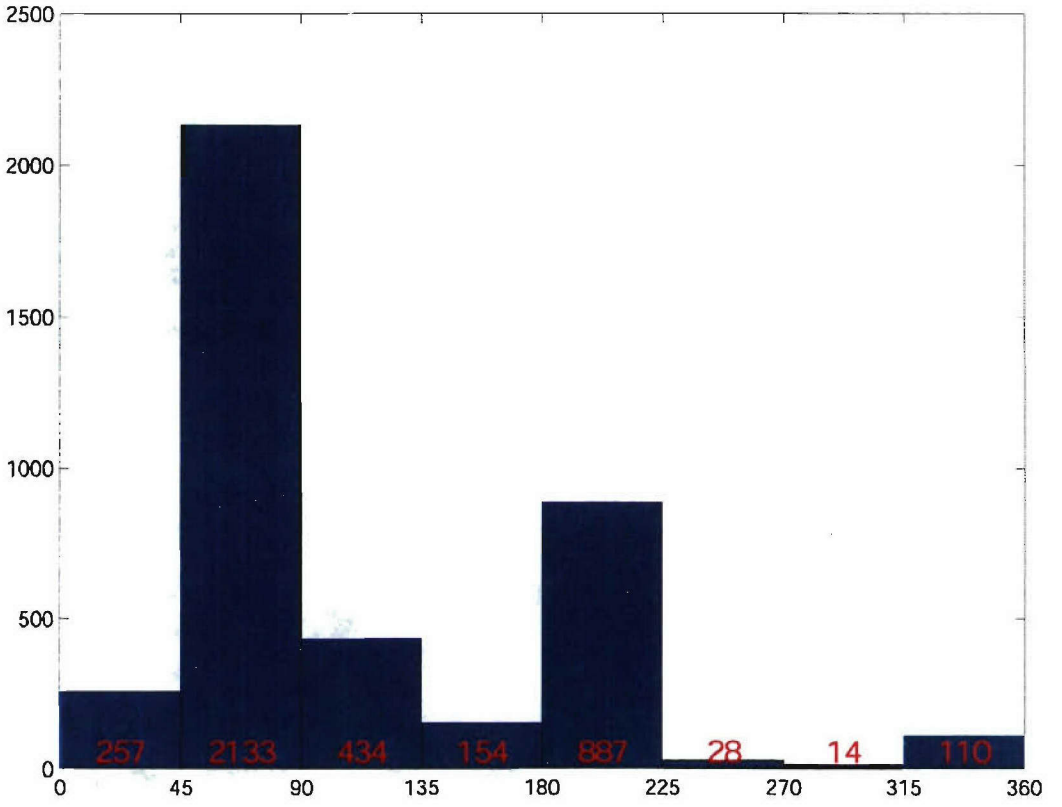

Figure A-29. As in Figure A-5 for months June, July, August 2003.

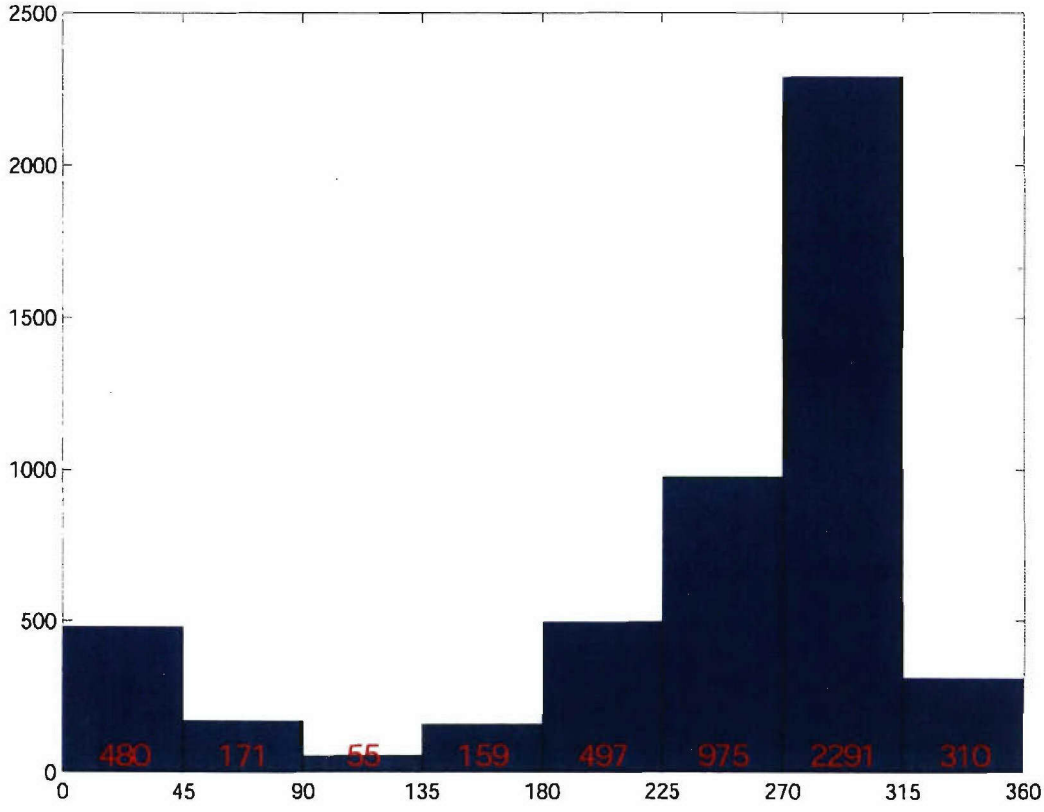

Figure A-30. As in Figure A-5 for months September, October, November 2003.

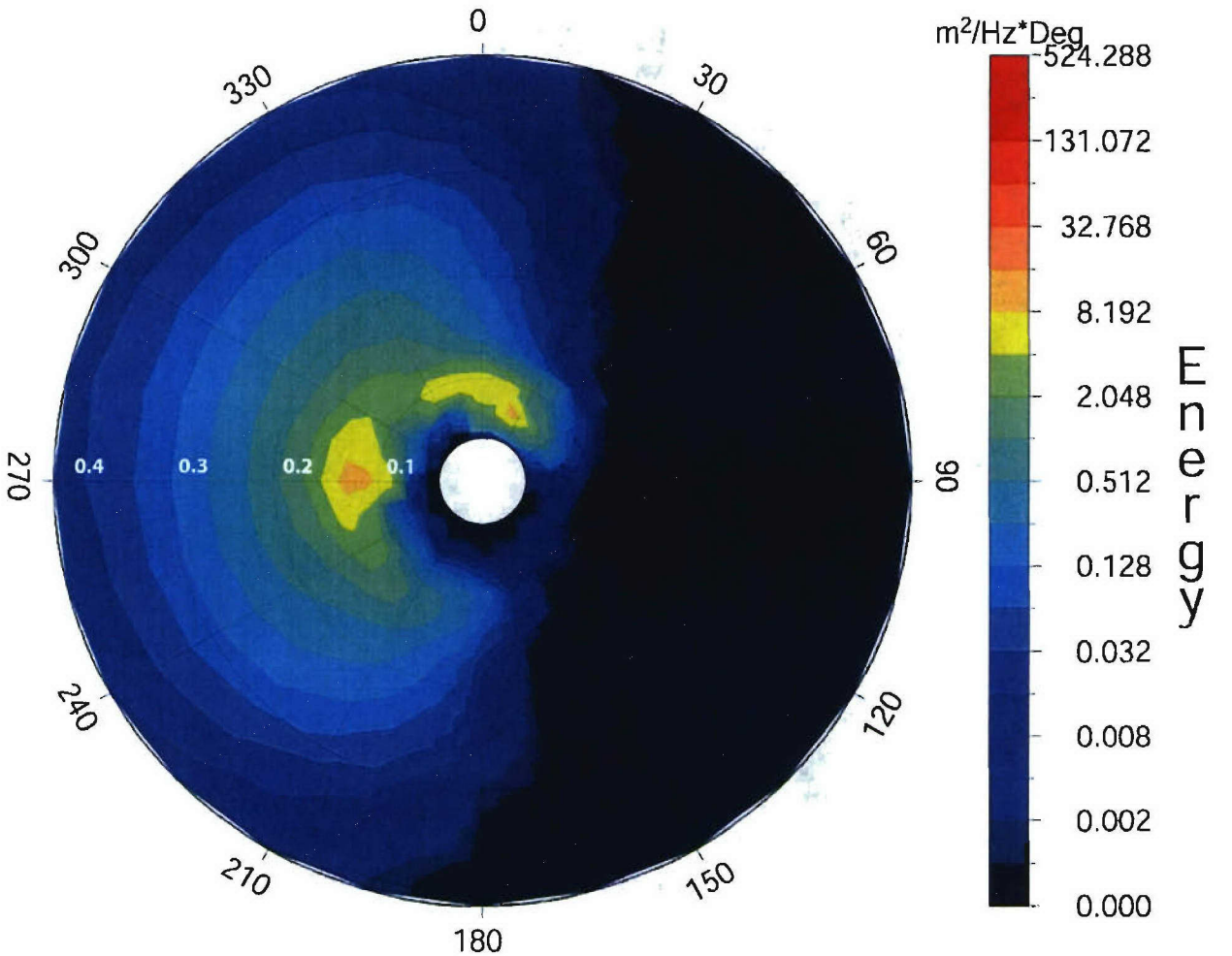

Figure A-31. Frequency, directional ocean wave spectrum for a grid point (38.00N, 170.00W) at 18Z on Jan. 4, 2003 in the wake region of the strong marine storm shown in Fig. 5. Frequency (Hz) decreases towards the center, wave energy scale (m^2/Hz*Deg) on the right hand side.

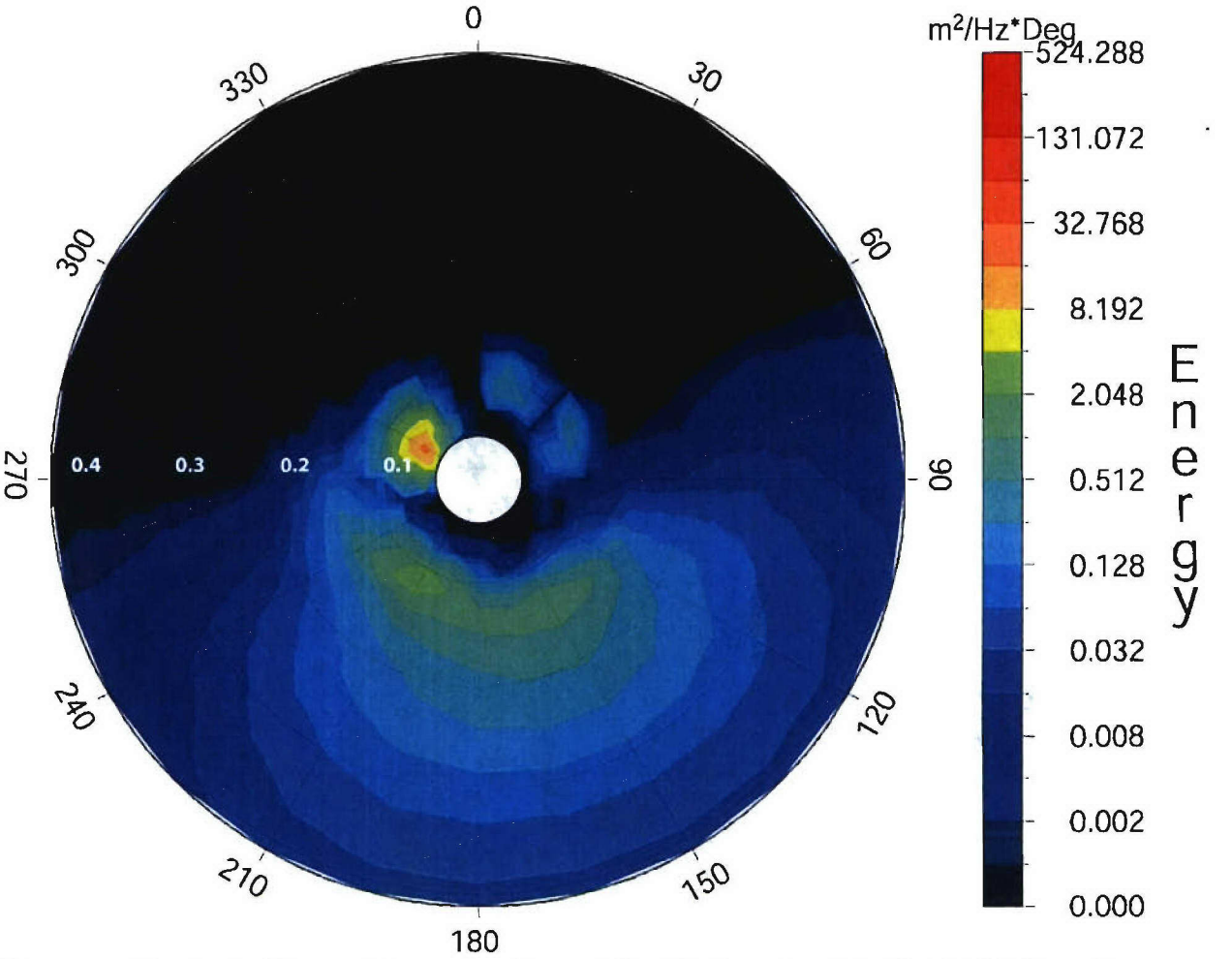

Figure A-32. As in Figure 24 but for Central Pacific location 0.00N, 153.88W on January 4, 2003 18Z (region of weak surface winds).

Figure A-33. Reflected and incident trade wind swells creating standing wave along a steep coastline of the Hawaiian Islands.

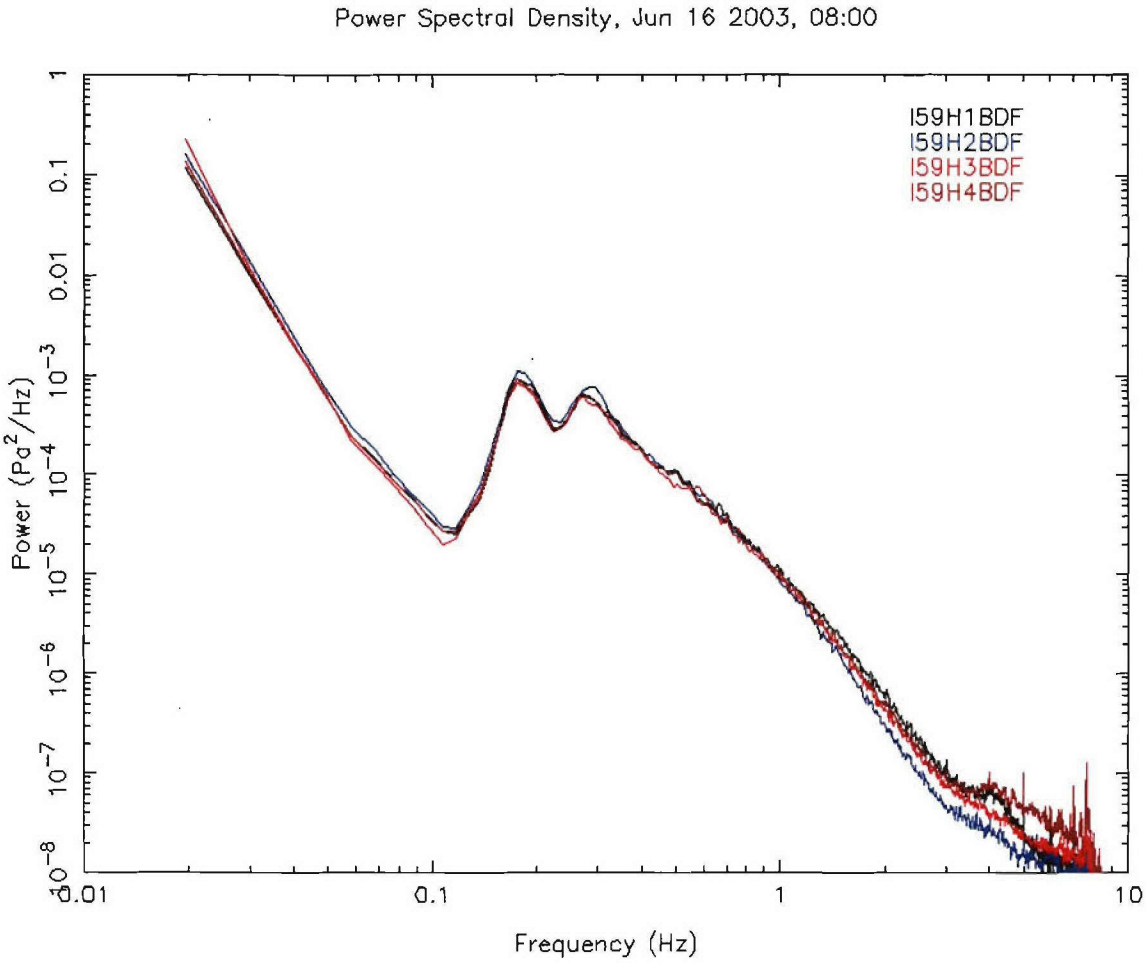

Figure A-34. Acoustic power spectral density observed at I59US site on June 16, 2003 18Z (8am Local). Colored lines represent power observed by the four components of the infrasonic array.

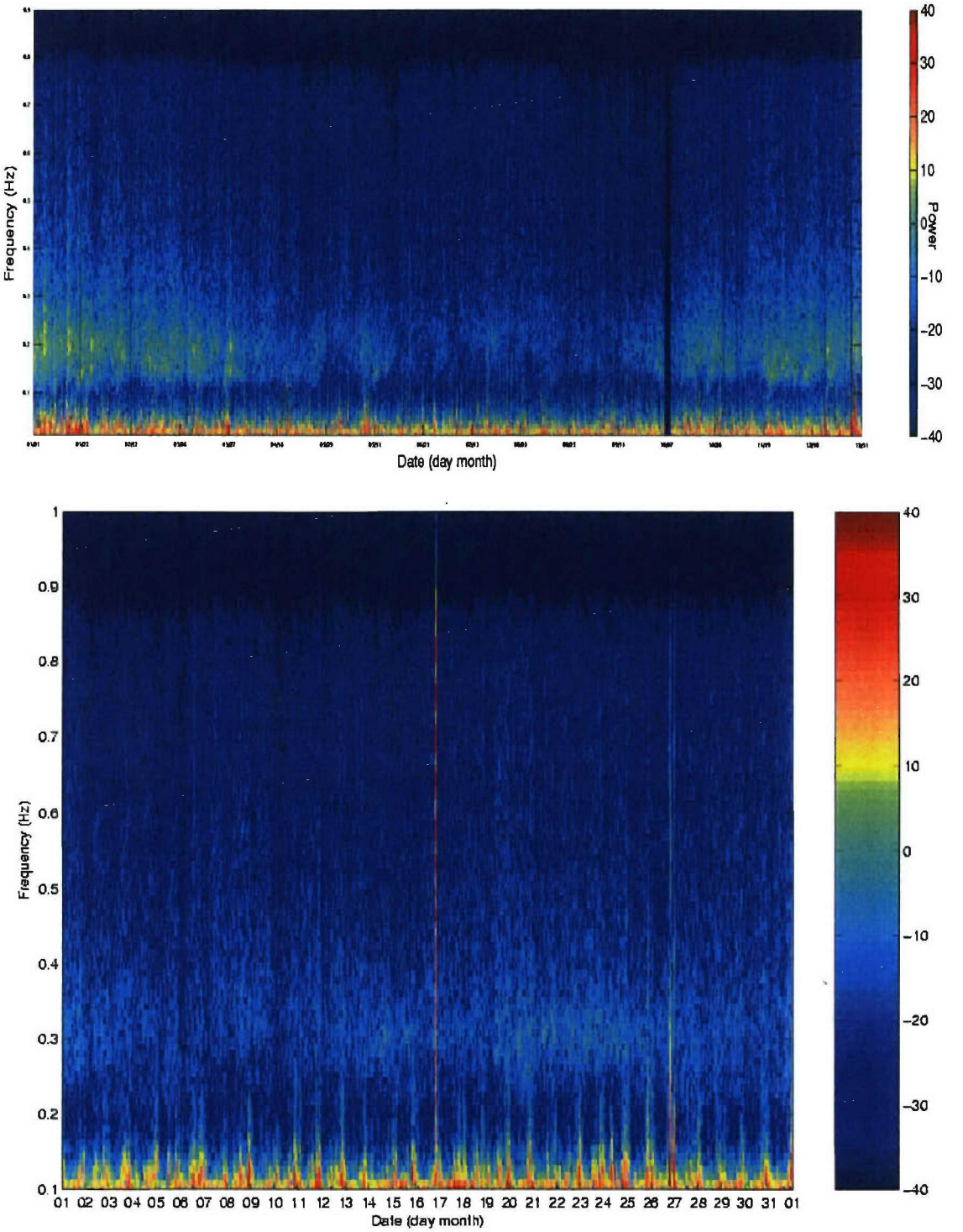

Figure A-35. Spectrogram for all of 2003 (upper panel) and January 2003 (lower panel) at IS59 in the 0.1-1 Hz frequency band. The upper panel shows the annual variability in the microbarom amplitude and frequency, whereas the lower panel shows the diurnal variability introduced by boundary layer wind fluctuations.

DEPARTMENT OF DEFENSE

DEFENSE TECHNICAL
INFORMATION CENTER
8725 JOHN J. KINGMAN ROAD,
SUITE 0944
FT. BELVOIR, VA 22060-6201
2 CYS ATTN: DTIC/OCA

DEPARTMENT OF DEFENSE CONTRACTORS

ITT INDUSTRIES
ITT SYSTEMS CORPORATION
1680 TEXAS STREET, SE
KIRTLAND AFB, NM 87117-5669
2 CYS ATTN: DTRIAC
ATTN: DARE

UNIVERSITY OF HAWAII, MONOA
INFRASOUND LABORATORY
73-4460 QUEEN KAAHUMANU
HWY., # 119
KAILUA-KONA, HI 96740-2638
ATTN: MILTON GARCES